



THE UNIVERSITY OF QUEENSLAND
A U S T R A L I A

FPGA packet filter with Ethernet MAC and web server using a RISC-V softcore processor

Thesis

Matthew Gilpin
45801600

2023

The University of Queensland
School of Electrical Engineering and Computer Science

Matthew John Gilpin
m.gilpin@uq.net.au

October 30, 2023

Prof Michael Bruenig
Head of School
School of Electrical Engineering and Computer Science
The University of Queensland
St Lucia, QLD 4072

Dear Professor Bruenig,

In accordance with the requirements of the degree of Bachelor of Engineering (Honours) in the division of Electrical Engineering, I present the following thesis entitled

“FPGA packet filter with Etherent MAC and web server using a RISC-V softcore processor”.

This work was performed in under the supervision of Dr. Matthew D’Souza. I declare that the work submitted in the thesis is my own, except as acknowledged in the text and footnotes, and that it has not previously been submitted for a degree at the University of Queensland or any other institution.

Yours sincerely,

Matthew John Gilpin

Abstract

This undergraduate thesis presents the design and implementation of both a hardware Ethernet Media Access Control (MAC) and packet filter on a Xilinx Artix 7 100T FPGA, specifically with the Digilent Artix 7 FPGA development board which includes a Reduced Media-Independant Interface (RMII) physical (PHY) interface chip. The primary objective of this work was to implement a firewall to improve security in the embedded systems space and to then host a web server on an onboard RISC-V softcore for configuration. More specifically, a NEORV32 RISC-V System on Chip (SoC) was used to interface the hardware over a Wishbone bus with the software hosting the webserver with FreeRTOS utilising both the Freertos-Plus-TCP and FreeRTPS-Plus-FAT libraries.

The wirespeed hardware five-tuple packet filter, analysing the destination IP, source IP, destination port, source port and protocol, showcased an added delay of just $4\mu s$ irrespective of packet lengths while potentially enhancing security over software based implementations. Many performance benchmarks were also conducted and concluded in a relative power draw of 0.51W including the microprocessor. In comparison other platforms such as the Nucleo-F767ZI, Raspberry pi Pico with WIZ5500 and MilkV-Duo were evaluated for their performance and efficiency.

In addition, the web server hosted a static single page application style website using Vue.js and Tailwindcss which was all stored on a microSD card and accessed over the SPI interface and using the FAT32 filesystem. UDP round trip times were also measured for all platforms resulting in an average delay of 1.45ms for the FPGA board which included an added 1ms delay.

Although effective, the packet classifier lacks support for IPv6 and only is applied to incoming traffic, while the firmware forgoes support for HTTPS. Given the FPGA's resource consumption of 11,738 slice LUTs and 12,505 slice registers, potential optimisations are discussed to overcome these shortcomings. A recommendation for future designs includes incorporating the efficiency and performance of the MilkV Duo RISC-V (CVITEK CV1800B based) board with an integrated hardware packet filter for a fast and secure embedded system platform.

List of Abbreviations

Abbreviations	
IoT	Internet of Things
CPU	Central Processing Unit
FPGA	Field Programmable Gate Array
PF	Packet Filter
MAC	Medium Access Control
ISA	Instruction Set Architecture
ASIC	Application Specific Integrated Circuit
SoC	System on Chip
TRL	Technology Readiness Level
IP	Intellectual Property
PHY	Physical layer
RMII	Reduced Media Independent Interface
CRC	Cyclic Redundancy Check
FIFO	First-In First-Out
LSB	Least Significant Bit
FSM	Finite State Machine
CLI	Command Line Interface
GUI	Graphical User Interface
RTOS	Real Time Operating System
RTT	Round Trip Time

Contents

Abstract	iii
List of Abbreviations	iv
Contents	v
List of Figures	viii
List of Tables	ix
1 Introduction	1
1.1 Motivation	1
1.2 Aim and Objectives	1
1.3 Scope	2
2 Literature review	3
2.1 Packet Filter Firewall	3
2.2 Field Programmable Gate Arrays	4
2.3 RISC-V processor	5
2.4 Computer Networks	6
2.5 Ethernet Media Access Control	7
2.6 Web servers and network stacks	9
3 Design overview	11
3.1 Hardware	11
3.1.1 FPGA	11
3.1.2 MicroSD card	12
3.1.3 System on Chip	13
3.1.4 Ethernet Media Access Controller	15
3.1.5 Packet Classifier	17
3.2 Firmware	20
3.2.1 Ethernet drivers	20
3.2.2 SD card drivers	21

3.2.3	Packet classifier drivers	21
3.3	Software	22
3.3.1	Real Time Operating System	22
3.3.2	Filesystem	22
3.3.3	Network Stack	22
3.3.4	Web application	23
3.3.5	Webserver	24
3.3.6	Command line interface	24
4	Results	26
4.1	Latency Performance	26
4.1.1	Theoretical analysis	26
4.1.2	Measured analysis	26
4.1.3	Improvements	27
4.2	Utilisation	27
4.2.1	NEORV32 processor	27
4.2.2	Ethernet hardware	28
4.2.3	Packet filter	29
4.3	Timing Summary	29
4.4	Filtering performance	30
4.4.1	Test setup	30
4.4.2	Test results	32
4.5	Comparison to preexisting solutions	33
4.5.1	Network latency tests	33
4.5.2	Network throughput tests	34
4.5.3	Security analysis	35
4.5.4	Firewall latency	36
4.5.5	Power consumed between boards	37
4.5.6	Thermal analysis	38
4.6	Power analysis	40
4.6.1	Theoretical power analysis	40
4.6.2	Measured power analysis	41
5	Conclusion	43
5.1	Limitations	43
5.2	Sustainability	43
5.3	Recommendations and future work	44
5.4	Summary	45
Bibliography		46

A Appendix	50
A.1 Neorv32 memory address space layout	50
A.2 FPGA primitives utilisation	53
A.3 Additional webpages built into the webserver.	53
A.4 UDP ping times between boards	53
A.5 Current measurements from boards	53
A.6 Thermal measurements for boards	53
A.7 Testing the firewall with 4 nodes.	54
A.8 Iperf 3 Test results	55
A.9 Eye Diagrams of PMOD port	55

List of Figures

2.1	Packet classifier	4
2.2	Updated Layers of the TCP/IP model	6
2.3	Network headers highlighting fields of interest of a UDP packet	7
2.4	MAC layer headers	8
2.5	An example Ethernet MAC FSM	9
3.1	Digilent Nexys A7 FPGA development board	12
3.2	MicroSD card used in project	12
3.3	System on Chip high level architecture	14
3.4	Format of frame in BRAM	16
3.5	8bit to 2bit FIFO used for RMII output	17
3.6	Memory Address Layout	18
3.7	Format of rules stored in BRAM	18
3.8	Packet classifier architecture	19
3.9	Format of SPI messages	19
3.10	SMI Write message structure	20
3.11	Screenshot of homepage on webapp	23
4.1	Added latency by packet filter waveform	27
4.2	Summary of the resource utilisation on XC7A100T FPGA	28
4.3	Critical path in SoC design	30
4.4	Network architecture for firewall tests	31
4.5	Average UDP RTT for different devices and payload sizes.	34
4.6	Software packet classifier timings	36
4.7	Comparison of Idle, Busy, and No eth currents for devices	38
4.8	Thermal images of boards under test after two hours	39
4.9	Post synthesis power summary for design	40
4.10	Zoomed in current consumption for ICMP pings	42
4.11	Current consumption of Nexys A7 with HTTP requests	42
A.1	Neov32 Memory Address space.	50

A.2	Screenshot of the about page in the webapp	52
A.3	Screenshot of the config page in the webapp	52
A.4	Nexys A7 and designed hardware Iperf3 test results.	55
A.5	Nucleo-F767ZI Iperf3 test results.	56
A.6	MilkV-duo Iperf3 test results.	56
A.7	Eye diagram of TXD through PMOD interface	57

List of Tables

4.1	Firewall configuration for testing	31
4.2	Summary of packets including expected and actual outcomes	32
4.3	Bitrate of various embedded devices	35
4.4	Temperature comparison of different chips during the test	39
4.5	Power consumption of components.	41
A.1	FPGA primitives utilisation for XC7A100T	51
A.2	Memory Utilisation	51
A.3	Slice Logic Utilisation	51
A.4	Average UDP RTT for different devices and payload sizes.	53
A.5	Device power consumption data (all values in mA)	53
A.6	Device measurements over time using FLIR One thermal camera, all measurements in degrees Celsius.	53

Chapter 1

Introduction

1.1 Motivation

In a technology era of increasing numbers of cyber attacks and record number of connected devices, ensuring these devices operate safely and securely is paramount. Consider the infamous Mirai botnet which strictly targeted IoT devices to become a part of their potent Distributed-Denial-of-Service (DDoS) network to cripple services such as Dyn (a DNS provider), Sony, Facebook, CNN among others like they did in 2016 [1]. In more recent years, the Australian Cyber Security Center (ACSC) received in excess of 76,000 cybercrime reports and growing in the 2021-22 financial year [2]. The growing trend of Internet of Things (IoT) will provide more opportunity for black hats (malicious attackers). IHS Markit estimates 125 billion IoT devices will be connected by 2030 [3]. This proliferation of IoT devices necessitates robust and adaptable security measures to counter the evolving threats posed by malicious actors.

To manage the surge of IoT devices, a shift to edge computing has emerged in favour of the traditionally more centralised cloud computing architectures. Edge computing as [4] puts it, is the paradigm which involves the computation and analysis of data at the *edge* of the network to be as close as possible to the source of the data. This has many advantages including: lower latency, lower bandwidth requirements, enhanced availability, energy efficiency, improved security and privacy [4]. Consequently, smaller and more efficient computers can be deployed at the edge/perimeter of these networks [5].

1.2 Aim and Objectives

To help alleviate the growing number of cyber attacks, this thesis aims to increase the security of IoT devices against cyber threads by designing and implementing a hardware firewall with Ethernet controller on an FPGA for use with a RISC-V processor. The work conducted in this thesis hopes to inspire future microcontroller/SoC designs to include hardware firewalls to help protect against cyber attacks.

The key objectives of this thesis are:

- Design and implement a hardware firewall capable of wire-speed filtering on an FPGA for IoT devices,
- Reduce the latency of hardware firewalls in embedded systems, ensuring packet classification adds the minimum possible delay after the relevant headers have been parsed, and to
- Establish a simple HTTP webserver on the RISC-V processor to facilitate user configuration of the firewall.

1.3 Scope

This thesis focuses on the core development of a hardware firewall and Ethernet controller with a RISC-V processor system. The scope of this thesis is limited to the following:

- Development of a 5-tuple binding packet filter for IPv4 networks to block unauthorised packets from reaching the microcontroller,
- Hardware design of Ethernet controller with integration to a RISC-V processor, and
- Configurability of the packet filter via a Web application.

Since cyber security is a broad topic and is constantly changing, this thesis will not cover all aspects of it. As such, the following topics are out of scope for this thesis:

- Protecting against all attacks,
- IPv6 packet handling and filtering,
- Deep packet inspection, and
- IEEE802.1Q VLANs.

Chapter 2

Literature review

This chapter introduces the necessary topics in relation to the project. These topics include, field programmable gate arrays, packet filter firewalls, RISC-V processors, Ethernet MAC, webs servers and network stacks.

2.1 Packet Filter Firewall

Usually, the first line of defence against bad actors, firewalls play a vital component in computer networks and as such can become vastly complex. In essence, the job of a firewall is to isolate and restrict access to an internal network from an external one to increase security [6].

There are several types of firewalls such as packet filters (PF), stateful packet firewalls and application firewalls [7]. Traditional PFs are considered as stateless and filter exclusively on the fields in the network and transport layer headers [7]. More information on the different layers in a network can be found in section 2.4. A five-tuple binding packet filter is an example of a stateless PF which filters on five key fields, source IP address, destination IP address, source port, destination port and protocol type.

Due to this, PFs are inherently simple, efficient and relatively effective in most situations. As a result, they are widely available and can be either implemented in software or in hardware [6]. The book, [6], also highlights some inherent flaws with PFs which include not being able to suppress sophisticated attacks and in some cases, can be challenging to properly configure. More advanced firewalls can perform deep packet inspection which explore the contents of the higher layers and factor in previous packets to better evaluate a packets true intention [7].

While firewalls such as *iptables* in Linux are software based, hardware acceleration can vastly improve the performance of a packet filter. As mentioned in section 2.2, hardware acceleration allows for parallelised algorithms to be executed independently of a central processing unit (CPU). Wicaksana and Sasongko, [8], proposed a packet classification engine as shown in figure 2.1. To obtain a fast yet reconfigurable and scalable packet classifier, the authors of [8] used a hierarchical tree-based algorithm that inspects the multidimensional fields of the IP header through the use of parallel decision trees.

Essentially, the architecture in figure 2.1 employs memory to store the ruleset and uses a multiplexer and a comparator to evaluate each of the fields in the header. As a safeguard, the authors opted for a *default-deny* ruleset to prevent any unwanted traffic. One inherent downside to this design is that it requires additional clock cycles for each rule that gets added to the ruleset.

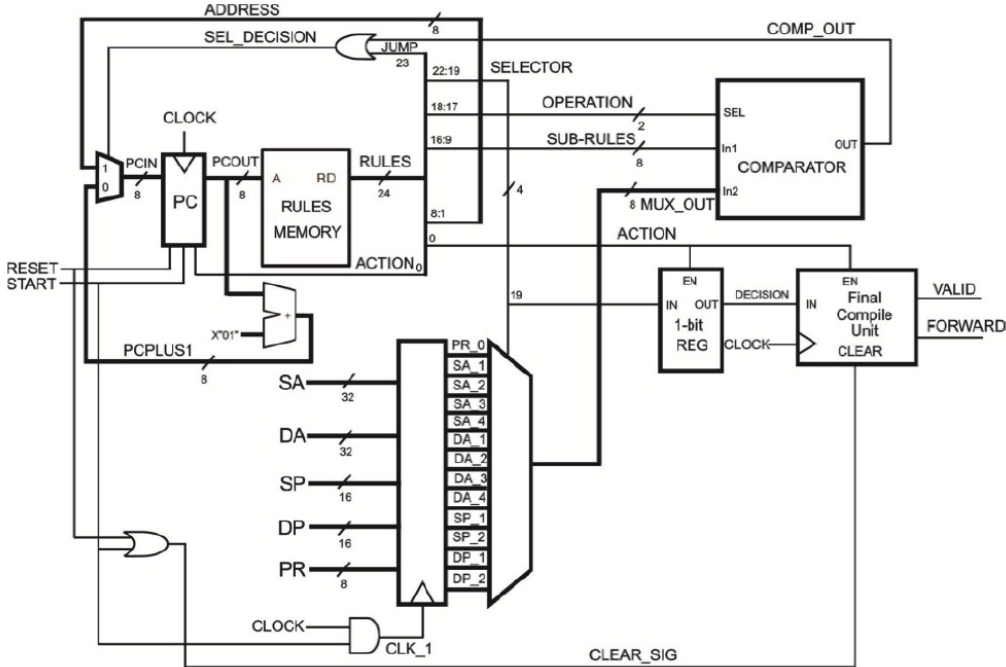


Figure 2.1: Packet classifier [8]

Wasti [9] presents several other classification algorithms for both hardware and software packet filters. '*Sequential matching*' provides the most trivial solution as it matches each rule to the incoming packet. While simple, this design has scalability issues as more rules get added. Another method proposed in [9] is by using a '*Grid of tries*' which uses tries (a type of tree data-structure) to help pattern match the packets, but fails to extend to multiple fields. Hardware algorithms using *Ternary CAMs* (stores words with 3-valued-digits - namely '0', '1' and '*') and *Bit-parallelism* were also discussed. Both of these exploited the parallelised nature of hardware design. One limiting factor with the classification methods cited in [9] is their configurability and expandability.

2.2 Field Programmable Gate Arrays

First introduced by Xilinx in 1984, field programmable gate arrays (FPGAs) allowed for large custom logic designs to be recognised without the need for expensive application specific integrated circuits (ASICs). More importantly, FPGAs did not suffer from the same scalability issues that programmable array logic (PAL) encountered and has allowed for larger and more complex designs [10].

A large advantage to custom logic is the ability to create highly parallelised designs with lower latencies and higher throughput than software-based serialised algorithms. This comes down to having a great degree of freedom when it comes to designing the architecture and ability to optimise for specific tasks. As such, FPGAs have become ubiquitous in both digital signal processing and

for accelerating an assortment of heterogeneous computing architectures and processes including networking [11]. More specifically, system on chip (SoC) design with custom hardware acceleration modules is an active area research. As [11] points out, there is a focus towards using both hardware and software in *edge devices*¹ due to growing numbers of IoT devices.

Several papers, [12] [13] [14], have proposed a range of related FPGA based firewalls that have different properties and focus on different optimisations. The key benefit to these firewalls is their high performance - namely, low latency, and high throughput. Article [12] proposed an Ethernet firewall using LwIP (A TCP/IP stack) with five-tuple binding (the five filtered parameters in packet filters) to achieve a throughput of 950Mbps with a latency of 61.266us. A conference proceeding in 2000 [13] used a comparator unit to check the fields of the IP headers obtained a filtering rate of 500,000 packets per second.

The enabling concept behind the above FPGA based firewalls is SoC design which involves integrating multiple components into a single package, or in this case a single FPGA. Often these will include small softcore microprocessors and some custom hardware such as Ethernet controllers or packet filtering hardware like the proposed designs in [12]. Having a microprocessor in the FPGA design can significantly reduce the complexity of the design and allows for quick and easy development in software instead of hardware [15]. In FPGA design, softcore processors are generally highly configurable and can be modelled in a hardware description language (HDL) which can then be synthesised onto ASICs or FPGAs hardware [15]. There are several softcore processor architectures available for FPGA designs including ARM Cortex, Nios II, MicroBlaze, and RISC-V.

While recently the royalty free RISC-V based cores have been popular amongst many SoC designs, other older processors are still common in the literature. The two big FPGA vendors, Xilinx (now AMD) and Altera (now Intel) have their own RISC based softcores. As an example, Janik et al. [16] used Xilinx's MicroBlaze processor as a media converter between optical (SFP interface) and copper (Ethernet) networks. Likewise, Altera's Nios II can be found in a variety of research papers including an embedded web server which significantly simplified the design [17].

2.3 RISC-V processor

There are four major processor architecture families, namely AMD64, x86, ARM and RISC-V. The two former instruction set architectures (ISA) are a part of the complex instructions sets (CISC) and are found in the majority of computers such as laptops and servers. ARM and RISC-V have a reduced instruction set compared to the CISC family and subsequently fall under the RISC family and are ideal for low power microprocessors [18].

RISC-V is an open and royalty free ISA and as a result, a plethora of softcore based custom implementations have been designed and are available for use in designs [19]. Consequently, there is an abundance of articles delving into RISC-V from evaluating the ISA [20] to creating multicore architectures [21]. A 2019 paper, [19] evaluated a variety of different RISC-V softcore processors.

¹*Edge devices* are a result of the edge computing paradigm which moves computation closer to the source [4]

RISC-V International have also published a list¹ of different RISC-V implementations that have a unique architecture ID. The majority of these are either written in a HDL for either application specific integrated circuits (ASICs) or FPGAs. The *NEORV32 RISC-V* softcore processor is written purely in vendor-agnostic VHDL and importantly has a considerable amount of documentation. The design is regularly updated by the maintainers with the original creator, Stephan Nolting, emphasising the importance of understandability.

Being a softcore processor, control is given over which modules are implemented. Some basic features of the *NEORV32 RISC-V* include UART, SPI, and GPIO interfaces [22]. The datasheet, [22], also mentions that it supports a '*Wishbone b4 classic*' external bus interface. A Wishbone B4 (or just 'wishbone') interconnection is designed specifically to connect modular pieces of hardware together on a SoC into the memory mapped 32bit address space in the processor [23]. This translates into accessing the hardware as a bunch of regular memory accesses like setting any other registers or values stored in main memory. This approach results in the benefit of not needing to create custom instructions for the microprocessor.

2.4 Computer Networks

To understand how one might go about creating an Ethernet interface and firewall, it is important to understand how networks operate. The TCP/IP model is a layered model that blueprints the different protocols and standards used in computer networks so that two devices can communicate in a prescriptive way. Figure 2.2 shows the updated five layers of the TCP/IP model mentioned in [24].

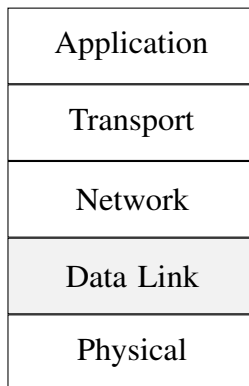


Figure 2.2: Updated Layers of the TCP/IP model

Each layer encapsulates the previous and provides a service to the layer above it. They are typically processed and handled by a separate process in either hardware or software. The physical layer is responsible for the transmission and reception of the above layers over a physical medium such as copper, radio frequency or fibre optics.

The data link layer (layer two, coloured grey) is responsible for the physical addressing of devices on the network and *links* devices together. Ethernet is the most common protocol used in the data link

¹See: <https://github.com/riscv/riscv-isa-manual/blob/master/marchid.md>

layer and will be discussed in 2.5 and throughout the thesis. Other protocols such as Point-to-Point Protocol (PPP) also exist [24].

The network layer (layer three) is responsible for addressing and routing of packets between networks and devices. The services this layer provides is one that is analogous to a regular postal service. The one major protocol used in this layer is Internet Protocol (IP) and it works by comparing known addresses in a routing table to the destination address of the packet [24]. RFC791 [25], defines all the protocol headers and how it operates.

The transport layer (layer four) is responsible for the end-to-end communication between devices and is where the TCP and UDP protocols reside. The application layer (layer five) is what is used for application specific protocols such as HTTP, FTP, and DNS.

Putting this all together a UDP packet can be seen in figure 2.3. The dark grey headers are the ones that are inspected in the five-tuple binding firewall. The trailing layer two FCS field has been omitted for simplicity.

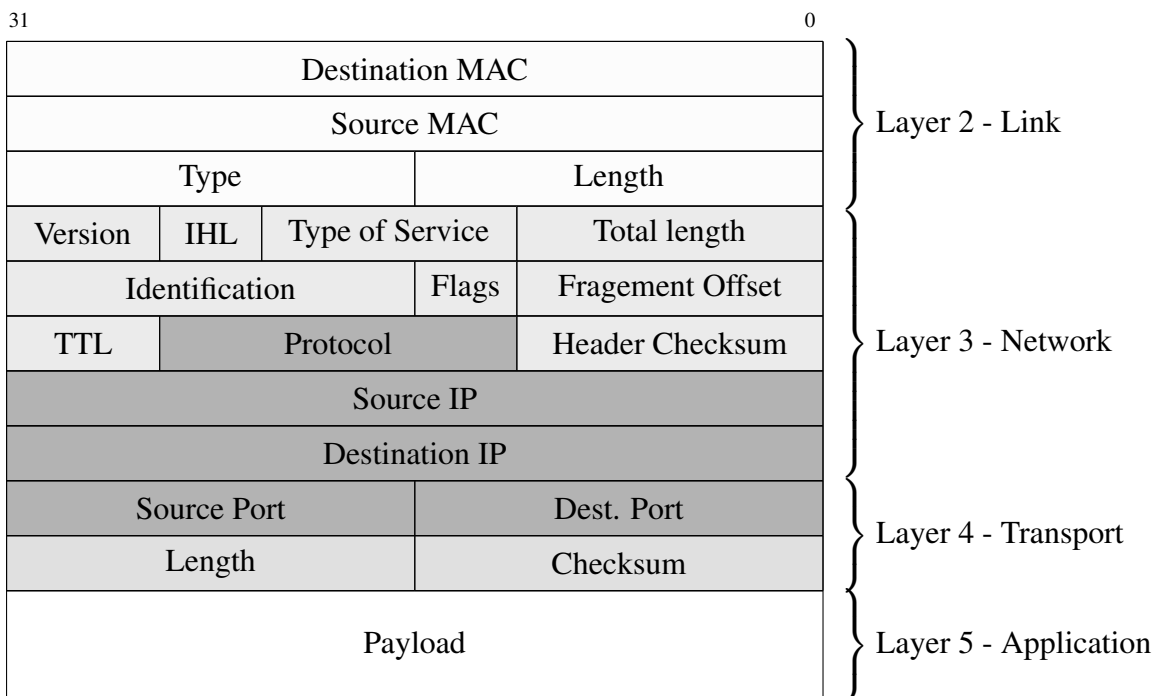


Figure 2.3: Network headers highlighting fields of interest of a UDP packet

2.5 Ethernet Media Access Control

First introduced in 1983, the IEEE 802.3 standard [26], more commonly known by the name of 'Ethernet', defines the '*Medium Access Control*' (MAC) protocol amongst other things for two or more devices to communicate over a network at layer two.

A core function of the Ethernet MAC is to attach the required MAC headers and preamble to the head and tail of the layer 3 payload to create an Ethernet packet. The fields in an Ethernet packet can be seen in figure 2.4.

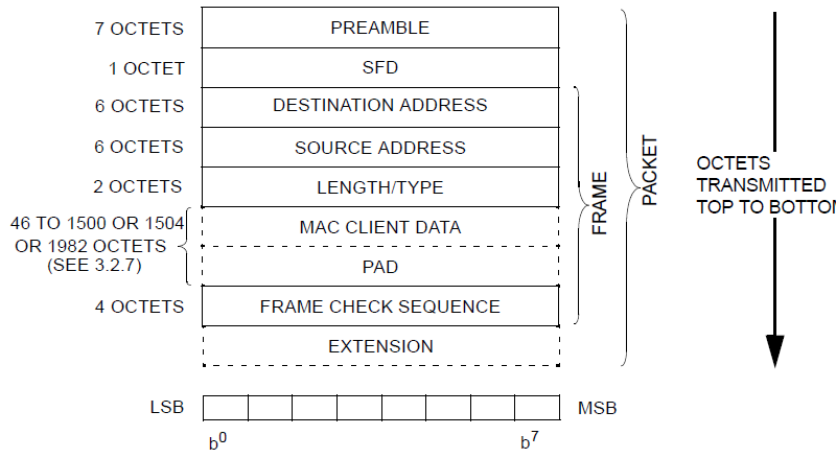


Figure 2.4: MAC layer headers [26]

The preamble and start frame delimiter (SFD) is used to synchronise the physical interface (PHY) and get it ready to send out data and is typically omitted when passing data up to higher layers such as for inspection with tools like Wireshark.

After the packet has been constructed, the data is forwarded to the PHY least significant bit (LSB) first [26]. Typically, a PHY management chip is used to handle the physical layer channel encoding and scrambling amongst other things. These PHY chips can often be interfaced with the media independent interfaces such as MII, RMII, GMII and RGMII [27]. The Reduced Media Independent Interface (RMII) is one of these standards defined in [26] and consists of a reference clock, 2 bit wide transmit (TX), 2 bit wide receive (RX) lines and a few other supplementary signals like defined in the LAN8720A datasheet, an example RMII PHY [28].

The MAC layer itself is usually implemented in hardware as it has several advantages over a software implementation. The core reasons behind this are due to parallelised nature of hardware and that parts of the MAC can operate independently [29] of each other. One key example is the calculation of the Frame Check Sequence (FCS in figure 2.4). The FCS for Ethernet is a 32bit cyclic redundancy check (CRC) [26]. CRC32 is not unique to Ethernet, but rather can be found in an extensive amount of applications. As such, prior research into parallelised architectures for the calculation have been made by others. Notably, Mitra and Nayak [30] proposed a low latency parallelised architecture for FPGA design on CRC32. As a result, packets can be assembled faster and offload additional processing burden from the CPU.

Numerous articles, [27] [31] [32], can be found about implementing Ethernet MACs on FPGAs each with a slightly different approach and focusing on different properties. Fundamentally though, as best highlighted in [27], a simple way of implementing a MAC is by employing a finite state machine (FSM) like the one in figure 2.5 to set the required fields and send out the packet. Another technique found in these articles is to use first-in first-out (FIFO) buffers to cross clock domains as the PHY speed likely won't match the clock frequency of the rest of the system. This is a common technique used in FPGA design as it allows you to have the packet assembly logic at a much higher clock rate than the output RMII reference clock speed [31].

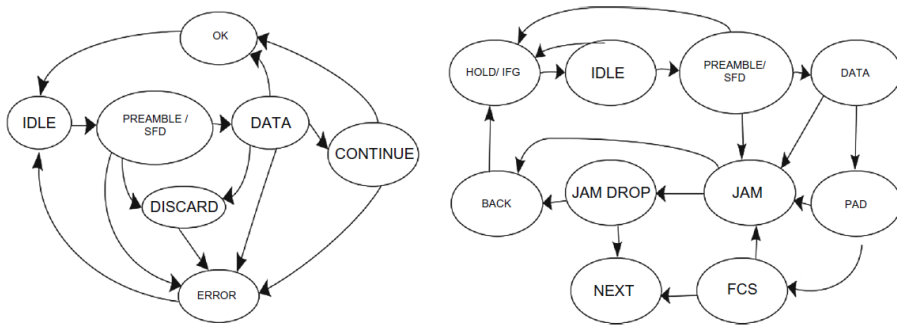


Figure 2.5: An example Ethernet MAC FSM [27]. Left: Receiver FSM, Right: Transmitter FSM

The source address field is typically filled in by hardware and is fixed as the MAC address is supposed to be globally unique to prevent address clashes on the same network. The destination address is typically set by software however as the ARP (Address Resolution Protocol) tables are typically stored in software due to them storing a mapping between the layer three IP addresses and the MAC addresses to forward a packet to.

The Length/Type field has a dual purpose, and it depends on the value. If a value is less than or equal to 1500, then it indicates the size of the packet. While if a value of greater than 1500, then it indicates the type of packet, called EtherType¹. Common values are 0x0800 for IPv4 packets and 0x0806 for ARP. Like with the destination address, this is usually populated by software as the type is dependent on the above layers.

In addition to the papers, there are a plethora of intellectual property (IP) blocks for xMII interfaces in HDL which have their own benefits and drawbacks. Some freely available HDL modules for Ethernet MACs can be found in both a complete^{1 2 3} and incomplete state⁴.

2.6 Web servers and network stacks

Almost all firewalls need to be configured with a ruleset which can be configured in two common ways, using a command line interface (CLI) or by a web-based graphical user interface (GUI). Before a web server can be realised, the network stack (Layers 3, and 4) need to be established since a web server operates at the application layer (layer 5). As embedded platforms are resource limited, special precautions need to be taken into consideration when it comes to memory and resource usage [33].

Article [12] investigated using the open source lightweight IP (LwIP) network stack as a mechanism for interfacing with the firewall. The LwIP library is a popular lightweight TCP/IP stack which has been investigated in a plethora of research papers and projects [34] [33]. Often these papers run LwIP on real time operating systems (RTOS) such as FreeRTOS or Zephyr. These provide an abstraction to the hardware that allows for multitasking and brings other OS-Like features to embedded systems.

¹See <https://en.wikipedia.org/wiki/EtherType> for the different types

¹See: https://github.com/yol/ethernet_mac

²See: <https://github.com/alexforencich/verilog-ethernet/>

³See: https://opencores.org/projects/ethernet_tri_mode

⁴See: https://github.com/pabennett/ethernet_mac

LwIP is not threadsafe and typically suffers from memory issues as found in [33]. However, FreeRTOS's own TCP/IP network stack called *FreeRTOS-Plus-TCP* provides a threadsafe Berkley sockets API and is newer. Consequently, less research can be found apart from existing documentation. These libraries typically implement multiple protocols such as DHCP, DNS, TCP, and UDP [35].

RFC2616 [36], defines the HTTP protocol used by all browsers and web servers and includes the formatting, allowed characters and the different request methods for each packet. HTTP1.1 and HTTP2 use TCP, typically on port 80, to communicate between the client and the server. However, HTTP3 uses the UDP protocol as defined in RFC9114 [37]. For the remainder of this thesis '*HTTP*' will be used to refer to HTTP1.1.

The HTTP specification, [36], defines the protocol as a stateless request-response type where the client first initiates a request to the server and the server responds with a status code and the requested data such as HTML data or images. *GET* and *POST* requests are the most common type and allow data to be retrieved and sent to the server. Since the browser renders the received HTML the data on screen, the webserver only needs to forward the raw HTML data (which can be stored on physical media) to the client.

Chapter 3

Design overview

This chapter details the design decisions and steps taken to complete the project. The project itself can be broken down into three main areas: hardware, firmware and software.

3.1 Hardware

3.1.1 FPGA

Digilent, parented by National Instruments, make a wide range of Xilinx based FPGA development boards and test equipment. In this project, the Digilent Nexys A7-100T FPGA development board (figure 3.1) was used due to it's availability and features including: a Xilinx Artix 7 100T FPGA (part number XC7A100T-1CSG324C), LAN8720A 100MBit/s RMII PHY, micro SD card slot and PMOD (auxiliary outputs) among other IO.

Xilinx has multiple FPGAs in their 7-series lineup with different target audiences. The Artix-7 family is optimised for low power designs with high logic throughput. The XC7A100T has 101,440 logic cells, 4,860Kbits of Block RAM (BRAM) and 240 DSP blocks [38]. There is a variant of the Nexys A7 FPGA board that consists of a XC7A50T FPGA (fewer resources), but ultimately the XC7A100T variant was used due to its larger amount of resources.

Importantly, there are four ways this FPGA can be configured (essentially '*programmed*'), at each power on cycle using JTAG, nonvolatile SPI flash, microSD card or using a USB stick through the HID interface. These modes are switchable using jumpers, JP1 and JP2, on the board. The JTAG interface is ideal for testing and as such it was used throughout development process, while storing these configurations on a microSD card was used once the design was solidified.



Figure 3.1: Digilent Nexys A7 FPGA development board.

3.1.2 MicroSD card

After the FPGA has been configured using the microSD card, the onboard microcontroller on the Nexys A7 board power cycles the microSD card and relinquishes control of the bus. On power up of the RISC-V softcore processor, it has full control of the card.

The selected MicroSD card for use in this project is the Patriot LX Series 32GB card, seen in figure 3.2. SD cards, like the patriot card have 2 modes of operation: native SDIO mode and SPI mode. While the native SDIO mode allows for higher speeds, it adds complexity to the design. As the files stored on the SD card are minimal (< 100KB), to keep things simple, the microSD card was connected in SPI mode.



Figure 3.2: MicroSD card used in project.

The files that were stored on the microSD card include the bitstream file for the FPGA itself and web assets for the webserver. While the bitstream file needed to be at the root directory of the filesystem, the web assets were stored in their own folder structure to help segregate the files.

3.1.3 System on Chip

A benefit to using an FPGA is that full control is given to the overall system design. At the heart of the SoC, a NEORV32 softcore processor¹ controls the hardware and runs the higher layers of the network and webserver tasks.

The NEORV32 processor is RISC-V compatible and designed by GitHub user *stnolting* and is highly configurable. In this design, seen in figure 3.3, the Wishbone, SPI, UART and external interrupts interfaces were enabled and configured. In addition to these, the M extension (Multiplier) was configured to use the DSP blocks to reduce the number of LUTs needed to handle multiplication in the core.

The Wishbone B4 classic bus is an open source interface that allows for multiple bits of hardware to connect and communicate together. In this project, the bus is 32bits wide and clocked at 80MHz, giving a bandwidth of $32 \times 80 \times 10^6 = 2.56 \times 10^9 \text{ bit/s} = 2.56 \text{ Gbit/s}$. Due to its relatively high bandwidth, it was used to connect the MAC with the NEORV32 as packets of 1500 bytes would need to be transferred quickly to not bottleneck the 100Mbit Ethernet interface. In addition to this, the MAC had an interrupt line to the NEORV32 processor to notify it when a packet has been received and ready for processing in the higher layers. This connects into the XIRQ lines which creates a fast interrupt request by firing a mcause trap event (RISC-V terminology).

Serial Peripheral Interface (SPI) was used to connect to both the MicroSD card and Packet classifier. These are comparatively low speed and low priority peripherals and so do not require a high speed interface. UART was connected to the onboard serial to USB converter chip for CLI commands and debugging.

¹See: <https://github.com/stnolting/nerv32>



Figure 3.3: System on Chip high level architecture.

Since the design is only concerned about incoming filtering, the packet filter was only placed between the RMII PHY and the MAC. By filtering at the RMII interface level, the Ethernet MAC is indifferent to the filter and ultimately doesn't care about it. This allows for a simpler modular design compared to integrating the filter in the MAC hardware. This filter consists of classifier (discussed in section 3.1.5) which would determine whether to forward or block an incoming packet.

To do the filtering itself, a shift register can be used to essentially delay the inputs from the RMII PHY until the packet classifier has determined whether to forward or drop the packet. A simple MUX can then be used to either allow the packet to enter the wishbone MAC or to not.

As the hardware in the MAC only processes the input if **crs_dv** is high, we only need to gate the **crs_dv** and can always have the **rxm** lines always attached. However, these should also go through a shift register.

By doing this, it means that we can operate the filter at wirespeed with the only downside is the

extra latency that the shift registers bring. The delay that these registers add to the latency can be found to be $T_{latency} = N \times T_{clk}$ where N is the size of the registers. In the design a size of 224 ticks was used. This is because at a minimum, the packet classifier needed to input a maximum of $22 + 24 + 4 = 50$ bytes (22 for MAC headers including preamble, maximum 24 bytes for IP header and 4 bytes for the TCP/UDP headers (only need to check the source and destination port)) need to be processed. As there are four clock cycles per byte the needed register size is $50 \times 4 = 200$ for the data to propagate to the end of the registers after the packet classifier has determined whether to drop or allow the packet. Importantly this does not effect the speed/bandwidth of the connection.

It is assumed that any traffic leaving from the device is safe and trusted. In a larger network where there are several devices behind the firewall, it may be desirable to also have a packet filter on the output.

3.1.4 Ethernet Media Access Controller

The advantage of using an FPGA is that custom hardware can be designed for specific tasks. In this design the MAC layer was done in hardware to free up the microprocessor by handling the lower level logic.

This MAC was implemented as a memory-mapped peripheral which used the MCU's Wishbone B4 classic interface. This then made it easily accessible over the memory address space of the MCU.

The hardware can be broken down into two main sections: the transmit logic and receive logic.

In the receive logic, there are two main functions, one that stores the incoming frame into BRAM and then another to interface the BRAM with the Wishbone interface. On the input side the data is shifted into a 8bit wide shift register - shown in figure 3.3. While `crs_dv` is asserted, after every four clock cycles (modulo four since 2 bits is received at a time) the contents of the shift register is stored into BRAM. After each byte has been added to BRAM, a counter is incremented to store the next byte in the next index. The end of the packet is signified when `crs_dv` is deasserted, at which point the payload length is stored for use when the processor receives the frame over the wishbone interface. After the first two bits equals "01" (first 2 bits of the preamble) have been received, a trigger output is asserted so that it can fire a CPU interrupt.

On the wishbone side of the receive logic, only read requests are accepted and processed. A register access returns the payload size of the received frame to help the driver (section 3.2.1) identify how much data it needs to extract from the hardware buffer. When accessing the BRAM memory locations over the Wishbone interface two things are considered. The first is that an offset of eight is needed since the BRAM stores the preamble and SFD which is not wanted by the processor. The second is that the payload is stored in 8bit values whereas the wishbone interface can send 32bits at once. Therefore some conversion between the memory addresses and the memory accesses to BRAM take place.

```

1 if wb_i_stb = '1' and wb_i_addr(31 downto 16) = x"1338" then
2     wb_o_ack <= '1';
3     if wb_i_we = '0' then -- Ensure write enable is reset to read.
4         if wb_i_addr(15 downto 0) = MAC_DAT_SIZE then -- Payload size

```

```

5      wb_o_dat <= std_logic_vector(to_unsigned(payloadLen, 32));
6  elsif wb_i_addr(15 downto 0) >= x"0008" and wb_i_addr(15 downto 0)
7      <= x"05F8" then -- BRAM access
8      virtAddr := to_integer((unsigned(wb_i_addr(15 downto 0)) - 8));
9      wb_o_dat <= FRAME_BUFFER(virtAddr) & FRAME_BUFFER(1 + virtAddr)
10     & FRAME_BUFFER(2 + virtAddr) & FRAME_BUFFER(3 + virtAddr);
11  end if;
12 end if;
13 else
14     wb_o_ack <= '0';
15 end if;

```

Listing 3.1: Wishbone access logic for Ethernet receive

By splitting the address over 2 if conditions, the amount of resources can be greatly reduced as the nested if conditions only need to compare 16bits instead of 32bits each time. Another important design decision is that this version of the Ethernet MAC does not validate the FCS after receiving a packet, instead it assumes it's a valid packet.

The transmit logic is broken down into three parts: Wishbone handler, main FSM and RMII conversion. The process of creating and sending an Ethernet frame starts with the processor sending data over the Wishbone interface. Like the receive logic, there are two types of commands that can be sent over the Wishbone interface, one that controls the logic, the other that stores payload data into BRAM. There are three configuration commands, one to initialise the hardware and FSM, another to start the transmission of data (used after all data has been transferred into BRAM) and one to set the payload length of the packet. The other register addresses allow the processor to store the payload in the frame buffer (BRAM). See figure 3.4 for the format of data in BRAM. The preamble, SFD and FCS are left out as these are appended in hardware. To be accurate, this is a quasi-MAC as the MAC addresses and type fields in the header (expanded view of payload in figure 3.4) are populated in software.

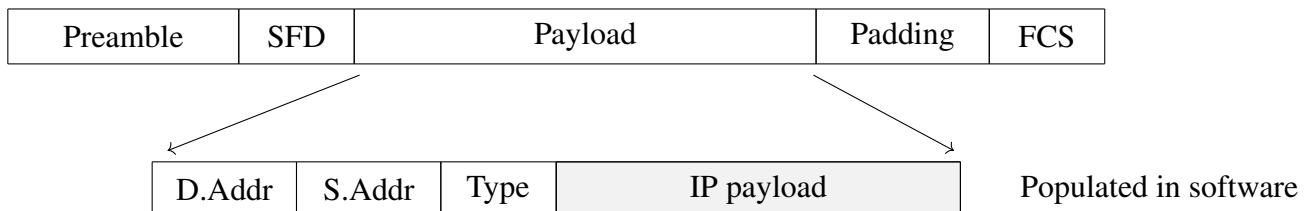


Figure 3.4: Format of frame in BRAM

Once a payload has been stored in the frame buffer, the main FSM takes control and at this point the CPU is free to do anything else. Since the FCS is calculated in hardware, the FSM resets the FCS hardware and begins to send the bytes to both the FCS hardware (to calculate the CRC32) and to a FIFO buffer. Once the payload has been transmitted to the FIFO, the resulting CRC32 FCS is sent out to the FIFO without missing a clock cycle.

A FIFO buffer is used to cross the domains since the RMII interface is 50MHz at 2bits wide, whereas the bytes are stored as 8bit vectors in the frame buffer. This also allows the FSM to have a higher clock speed as well. The current implementation of the FSM uses a 80MHz clock signal, consequently the equivalent bit rate is 6/4 times larger than the output needed to the RMII interface. The FIFO used in this design, figure 3.5, is slightly modified so that the read clock is one quarter the 50MHz output frequency since the FIFO itself returns 8 bits at a time. An FSM operating at 50MHz then sends each 2bit nibble out to the RMII PHY at a time in a circular fashion. The tx_en line is asserted while the FIFO is non-empty.

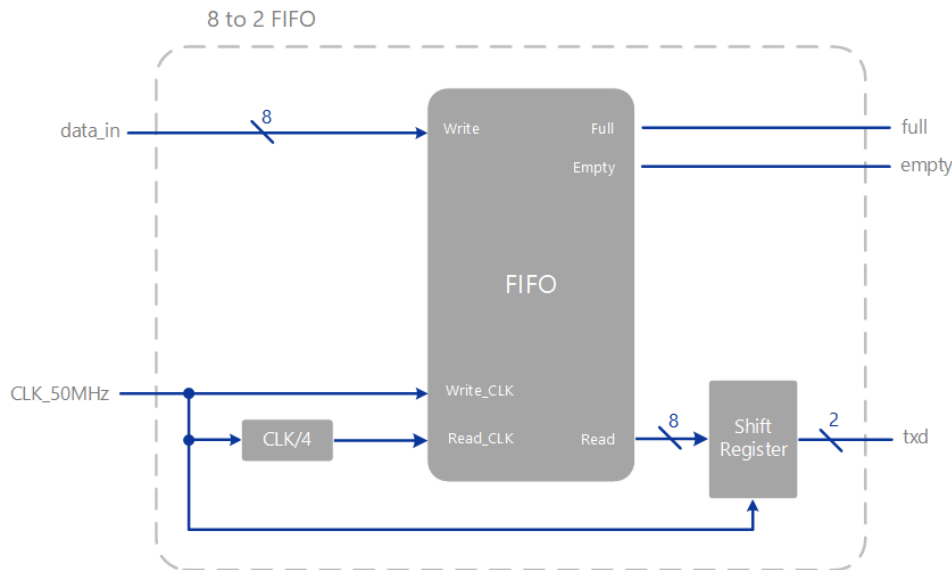


Figure 3.5: 8bit to 2bit FIFO used for RMII output.

The documentation for the NEORV32 states that all memory accesses that do not target specific processor-internal address regions (see appendix A.1) get forwarded to the external interfaces, such as the Wishbone interface. As such, there is a large block of unused memory between the IMEM and DMEM regions. The memory mapping, figure 3.6, used in this design ranges from 0x13370000 to 0x133805F8.

This mapping is required for developing the driver (section 3.2.1) to access the correct registers.

3.1.5 Packet Classifier

To further save MCU resources, the packet classification was done in hardware. Not only did this reduce the load on the MCU itself - giving it more time to do other things - it allowed the interface to run at '*wirespeed*'. That is, at the full speed of the interface - 100Mbit/s.

This was possible by having the ruleset been evaluated in parallel as the data is coming into the firewall. This method however is not suitable for large rulesets as the fan-in and fan-out limit the maximum number of parallel comparisons. For every new rule, the number of gates grows exponentially. Hence a design decision of a maximum ruleset of size 8 was chosen.

The way this classifier was designed was to be a '*default-block*' where all connections were blocked except for the ones specifically whitelisted in the ruleset. The specific rules had a few options, namely

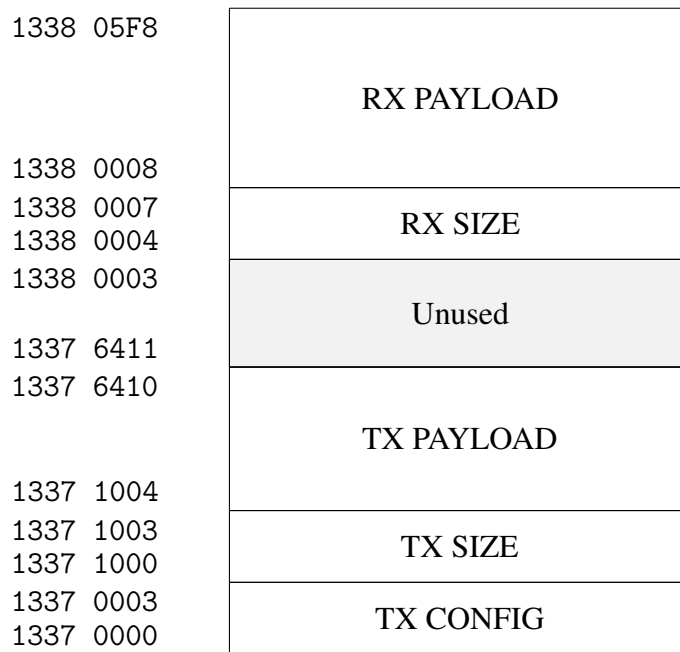


Figure 3.6: Memory Address Layout

the source IP address, destination IP address, source port, destination port and protocol could be configured. In addition to these, each field had a wildcard operator which allowed all values for that specific option to be classified.

The design of the packet classifier hardware, figure 3.8 stores the firewall rules in block memory. The rules are stored in BRAM as an array of 112 bits with the format shown in figure 3.7.

Wildcard	IP_{Dest}	IP_{Src}	$Port_{Dest}$	$Port_{Src}$	Protocol
----------	-------------	------------	---------------	--------------	----------

Figure 3.7: Format of rules stored in BRAM

The wildcard attribute signifies whether to allow all possible combinations (in other words, disregard) for the positional attribute where the most significant bit refers to the IP_{Dest} and the least significant bit refers to the *Protocol*.

A FSM then records the position of the incoming and configures the multiplexers on the BRAM to output the current property to the comparators where they compare with the shift register which contains the current field being classified. On a successful match, a bit is left set in the result register, otherwise clear if no match. Importantly, the bits only get set on the first iteration of the classification.

After passing through all the fields, if there is any bit set in the results register, it indicates that a rule matched and that a packet should be forwarded.

This reduces the required resources as only 1 set of comparators are needed, which is important as for each rule that exists, another comparator is needed. In this design, there are a total of 8 comparators, 8 multiplexers and the results register is 8bits wide.

A more resource efficient design is possible at the cost of latency. This is one of the critiques of the design mentioned in [8] as multiple clock cycles would be needed to classify the headers. In theory

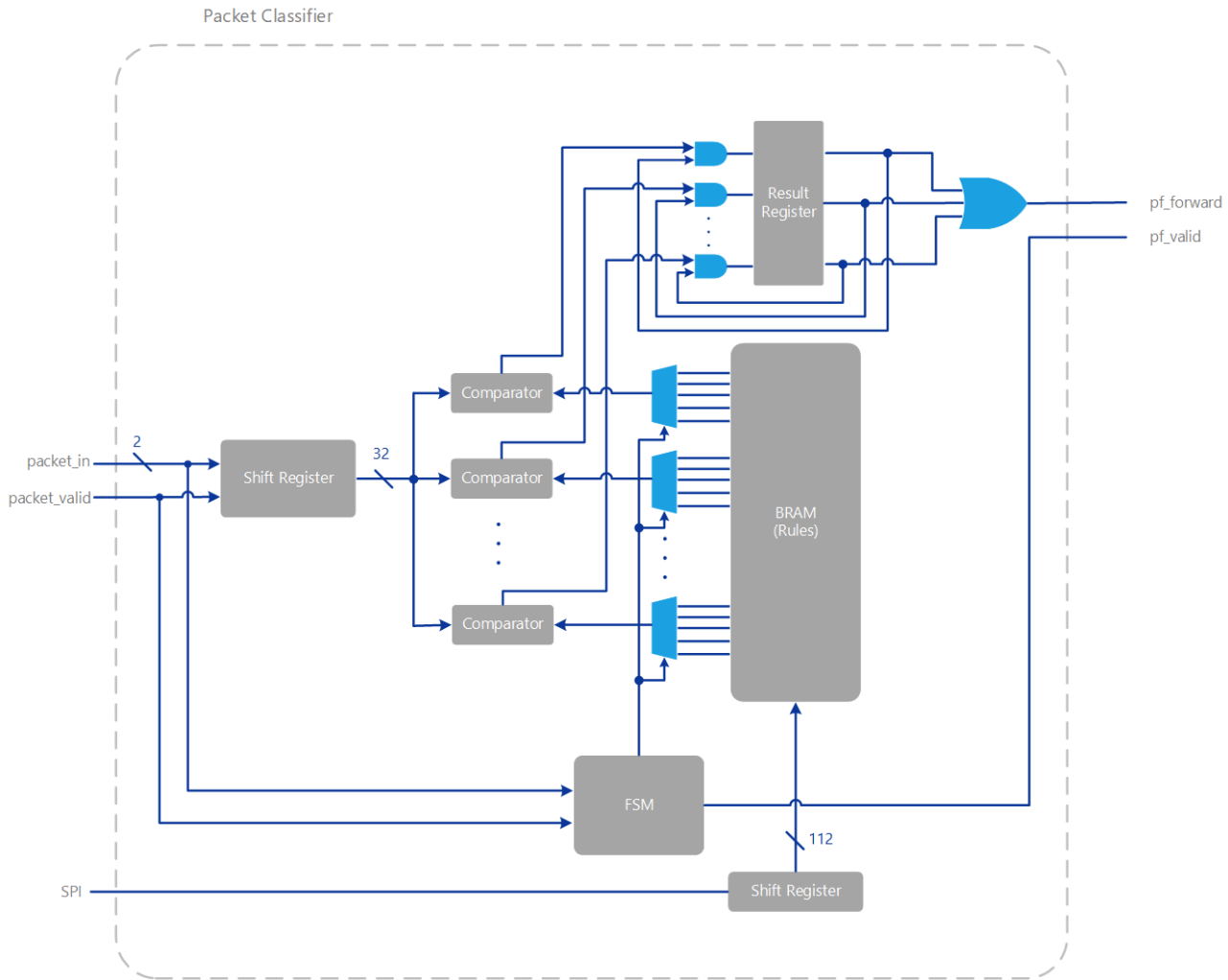


Figure 3.8: Packet classifier architecture. Clock signals have been omitted.

the clock speed could be faster than Ethernet frequency and as only two bits from the RMII interface are processed at a time, it could be a viable alternative, however this may likely fall apart when higher speeds are required.

Several options exist for configuring the ruleset in the packet classifier such as: Wishbone, I2C, UART, SPI or a completely custom solution. For simplicity, SPI was used in configuring the packet filter. Importantly, data would only flow in one direction, from the microcontroller to the classifier and not the other way round. This means that the microcontroller needs to keep the state of the rules inside the packet filter and needs to resend the rules to be sure of the configuration. This is not an issue as the rules need to be stored in flash on the microSD card to keep settings between power cycles. The format, figure 3.9 that the SPI hardware expects is similar to how it's stored in BRAM to make it quick and easy to transfer.

<i>Index</i>	<i>Wildcard</i>	<i>IP_{Dest}</i>	<i>IP_{Src}</i>	<i>Port_{Dest}</i>	<i>Port_{Src}</i>	<i>Protocol</i>
--------------	-----------------	--------------------------	-------------------------	----------------------------	---------------------------	-----------------

Figure 3.9: Format of SPI messages

Notably, the data is received into a shift register and after all bits have been received the BRAM is updated at the corresponding index in a single clock cycle.

3.2 Firmware

3.2.1 Ethernet drivers

Since the Ethernet hardware was custom, drivers were needed to interface with the hardware in software. There were two types of commands that were needed, first the RMII serial management interface (SMI) and secondly the MAC drivers - the drivers that would handle the data. The SMI interface is used to control the mode of operation of the PHY chip including the speed, Auto-MDIX, duplex settings. The LAN8720A datasheet, ([28]) provided some details (seen in figure 3.10) into how the protocol operated. The datasheet also outlined that a maximum frequency of 2.5MHz, but no lower bound. As such the interface was '*bitbanged*' with GPIO pins to reduce complexity. The maximum switching frequency of the NEORV32's GPIO was measured to be $\approx 1\text{MHz}$, thus no additional delays were needed in the code and that the GPIO pin could be toggled at the fastest speed possible.

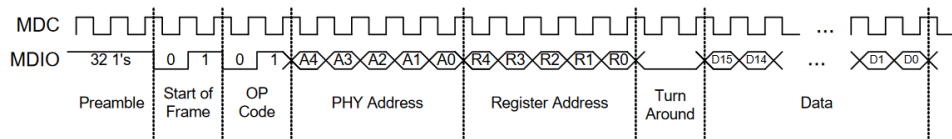


Figure 3.10: SMI Write message structure. [28]

On power up the RMII interface would be set to full duplex, 100Mbps and auto-negotiate in accordance to the LAN8720A datasheet. 10Mbit and half duplex modes were excluded from the design as further hardware design would be required.

As the Ethernet hardware used the Wishbone interface, the register locations were mapped into the processors address space. Accessing these registers is analogous to accessing any other variable in memory, using pointers to the memory address. As an example, to access memory location `0x12345678` the following C code can be used `*(volatile uint32_t *)0x12345678`

To simplify the design and improve readability, a range of macros was setup, such example of macros can be seen below.

```

1 #define ETH_MAC_TX_BASE 0x13371000
2 #define ETH_MAC_CMD_BASE 0x13370000
3
4 #define ETH_MAC_CMD  (*(volatile uint32_t *)ETH_MAC_CMD_BASE)
5 #define ETH_MAC_TX ((EthMacTx *) ETH_MAC_TX_BASE)
6
7 typedef struct __attribute__((__packed__))
8 {
9     volatile uint32_t SIZE;
10    volatile uint32_t DATA[375]; // 1500 / 4 = 375.
11 } EthMacTx;
```

Listing 3.2: Python example

This allowed for the connected wishbone Ethernet to be accessed like any other register in the embedded system.

There are three fundamental functions that the driver itself must fulfill, initialisation, send data and receive data. The initialisation resets the Ethernet MAC and resets the interrupt registers.

The send method is also trivial, but importantly it takes in two parameters, the first is an array of data to send and the second is the amount or length of the data. Like with the SMI interface, these instructions and data transfers were actioned without any delays as the hardware was capable of handling the native speed of the processor. After the data had been transferred, the hardware is instructed to send out the packet. There is no need to provide the FCS as this is calculated on the fly in hardware.

Similarly, a receive method was created that took in a buffer to store the bytes into as it transfers the data into memory from the registers. Both the transmit and receive functions handled the data translation from 32bit values over the wishbone interface to 8bit bytes in software. In addition to this, as the Ethernet hardware used external interrupts to signal to the processor that there is an Ethernet packet ready for processing. This would use direct task notifications to signal to other functions in the code to call the receive method.

3.2.2 SD card drivers

To use a micro SD card, drivers must be created so that the card can be initialised, written to and read from. More precisely, in accordance to the documentation for the FreeRTOS-Plus-FAT file system, the driver had to implement a function that reads sectors from the media and one that writes sectors to the media.

Unlike the Ethernet MAC, initialising a MicroSD card isn't as trivial and requires multiple steps. A guide online for AVR¹ was followed and the code was ported to the NEORV32 system. In a nutshell, the SPI interface was initialised with a clock divisor of 1 and a prescalar of 3, several commands were sent and received from the SD card and then it was put into IDLE mode after increasing the speed of the SPI interface to have no clock divisor and a prescalar of 1.

Similarly, the same guide was followed to implement the read and write sector functions. Importantly, these functions would read and write a whole block at a time. On a microSD card, a block is considered to be 512 bytes.

In addition to these, a simple function to determine if a SD card is present in the slot was also implemented to warn the user if data was attempted to be written to or read from without a physical card in the slot.

3.2.3 Packet classifier drivers

An initialisation function was created to enable and configure the SPI interface on the microprocessor for mode 0, and with no clock divisor and a prescalar of 1. The SPI hardware for the classifier can handle speeds in excess of 80Mhz (seen in section ??), hence there was no need to slow down the

¹See: <http://www.rjhcoding.com/avrc-sd-interface-1.php>

clock. Moreover, calling this initialise function is only required if the microSD card intialise function has not been called.

A single function was created that takes in all the attributes needed in the packet filter and that sends these out in the correct order and format to the hardware.

3.3 Software

3.3.1 Real Time Operating System

In addition to simplifying the software, an RTOS was used to allow the use of network TCP stacks and handle multiple concurrent connections at a time. FreeRTOS version V10.4.4 was used due to its familiarity and compatability with the NEORV32 MCU. FreeRTOS also had integration with their own filesystem (section 3.3.2) and TCP/IP stack (section 3.3.3).

3.3.2 Filesystem

The FreeRTOS-Plus-FAT filesystem library was used to allow the system to read and write files (such as web assets) to a microSD card. The library is managed by FreeRTOS and is DOS compatible which allows FAT32 formatted drives to work. Other popular filesystem modules such as FatFS¹ and LittleFS² were also considered, but did not have the same level of integration and active support as the FreeRTOS option.

The library then uses the microSD card drivers (section 3.2.2) to access the disk.

3.3.3 Network Stack

Two main options for the network stack were available, LwIP and FreeRTOS-Plus-TCP. The main concern with LwIP was that it was not threadsafe and had memory issues. In addition to this, as FreeRTOS was chosen as the RTOS, their own TCP stack had tighter integration. The stack provides a Berkeley sockets API which is the same used in full-blown operating systems such as Linux. It also includes support for ARP, DHCP, DNS and ICMP protocols, which were used throughout this project.

Like with the filesystem library, the stack needed to be ported to the NEORV32 processor and importantly the custom Etherent hardware. In addition to the transmit, receive and initalisation methods, functions to return random numbers were needed. These are for the TCP sequence numbers and are required to truely random for security. As such, the hardware based true random number generator in the NEORV32 core was used.

The network stack was configured to use DHCP to automatically aquire an IP address from a DHCP server on a network so that when it's transported between networks it can dynamically get a new IP address and can be accessed without needing to reconfigure the device. The device can then be

¹http://elm-chan.org/fsw/ff/00index_e.html

²<https://github.com/littlefs-project/littlefs>

given a static IP through the DHCP server by creating a static mapping. This will then prevent the DHCP server from assigning the desired IP address to another device accidentally.

3.3.4 Web application

With the resource constraints of the RISC-V microcontroller in mind and other design requirements, Vue.js was chosen as the framework of choice for developing the web application in. Vue.js is a framework for developing componentised single page applications. Although technically single page, the javascript it compiles handles routing between web pages on the client side in javascript. This means that once the initial page has loaded, no additional server requests need to be made to change page. To make the website appear dynamic, an API can be used to fetch data and statistics from the device itself. These HTTP API requests are much smaller than the requests needed to load the webpage initially. This results in very low network traffic between the client and server, perfect for embedded systems.

For styling, Tailwindcss was used to help style the webpages to give the webapp a contemporary feel.

The webapp consisted of 3 main pages, the index or home page, about page and config page. The home page, figure 3.11 showed statistics such as total and blocked packet count, and statuses for a few tasks on the microcontroller. These tasks, through an API call, can be toggled on and off to save resources. An uptime reading is also present. These values are updatable by clicking the 'refresh' button.

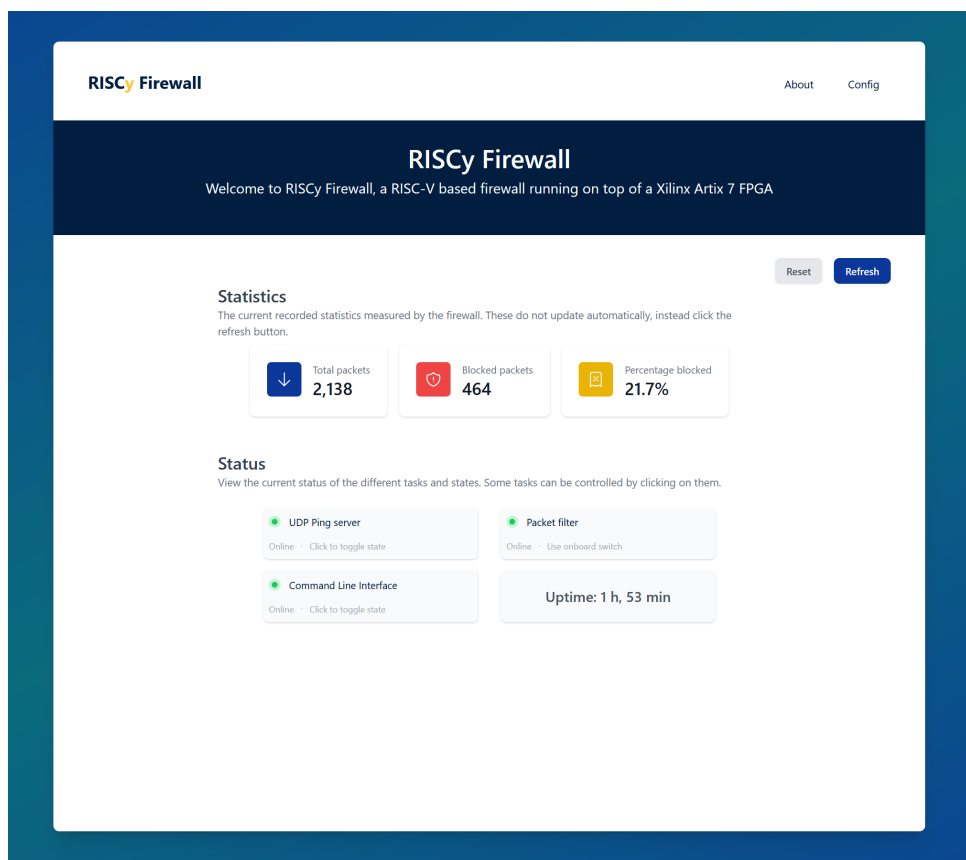


Figure 3.11: Screenshot of homepage on webapp.

The configuration page, (figure A.3 shown in appendix A.3) is where the user configures the firewall rules. The rules first need to be loaded which is requested through an API request. This API request reads the rules from the microsd card, sets the rules (for consistency) and then returns them in the response packet. When the user saves a set of rules, an API request is made which first applies the rules and then saves the rules to the microsd card so that the changes are persistant.

An about page (figure A.2 shown in appendix A.3) was also created for demonstration purposes and contained an image.

In addition, as this is all client side and compiles to html, css and javascript, no special webserver is required for things such as server side rendering.

3.3.5 Webserver

A simple HTTP webserver running on top of a TCP server was used to serve the webpages for the project. FreeRTOS give an example of how to setup a TCP and HTTP server that uses the FAT filesystem to get the content such as the html, css and javascript files. All the TCP webserver has to do is determine the route requested by the client, based on this it knows whether to read a file from the micro SD card and send it over multiple TCP packets or if it needs to respond with raw data like in the case of the API. Regardless of the type of request, a response is formed in the standard HTTP 1.1 format given in RFC2616 [36].

3.3.5.1 API server

A subset of the webserver is the API server itself. To make the design simpler, an API was created so that the interface to set and get the firewall rules was independant of the web content. The way the software distinguishes between requests to load a webpage and the API server itself is by inspecting both the route/URL (pcUrlData) and the method type (GET, POST, PUT).

For setting the firewall rules, a POST request to the '/api/firewall' endpoint can be made. The body of the request would contain the rule in the following format

$$payload = Index|Wildcard|IP_{Dest}|IP_{Src}|Port_{Dest}|Port_{Src}|Protocol$$

Where | is the concatenation operator and all fields are in hexadecimal. As an example, to insert a rule at index 0, and with a wildcard operator for all items with a destination IP of 10.20.1.120, source IP of 10.0.0.159, source and destination port of 80 and a protocol of TCP, the following body would need to be sent to the API: `payload=003F0A1401780A00009F0050005006`. The API server then takes the necessary action and applies the rule to the packet filter by calling the methods in the packet filter driver (section 3.2.3).

3.3.6 Command line interface

To aid with debugging the FreeRTOS-Plus-CLI framework was used. This would easily allow certain actions to be executed on demand without the need to reflash or reset the device each time. Such

examples include configuring the PHY, ethernet MAC, sending ICMP packets and filesystem related commands. In addition, the firewall rules can be set from the CLI in the event that the firewall blocks HTTP connections.

Chapter 4

Results and Discussion

This chapter aims to demonstrate the practicality and efficacy of the designed hardware. Performance metrics such as latency, resource utilisation, timing, and power consumption are analysed to gauge the design's effectiveness. The design is also tested with a small sample of real life packets of different properties to ensure the packet filter can correctly block unwanted packets. Preexisting solutions are then compared with the design, providing insight into the design's relative strength and weaknesses in areas of latency, power and thermal performance.

4.1 Latency Performance

Reducing the latency of hardware packet filtering in embedded systems is one of the key objectives of this thesis. As such, verification of the latency added due to the filtering is essential.

4.1.1 Theoretical analysis

The design employs a 200-stage shift register to temporarily store the incoming packet with each stage being 2bits wide. Given a clock frequency of 50Mhz, the added latency can be calculated to be $200 \times \frac{1}{50 \times 10^6} = 4 \times 10^{-6} = 4\mu s$.

4.1.2 Measured analysis

The packet classifier's performance was measured with an Agilent MSO6054A MSO due to its high sampling rate of 4GSa/s. A PMOD pin was connected to output of an xor operation between the carrier sense line (crs_dv) from the PHY and the crs_dv post packet filtering.

This process allowed the added latency to be measured characterised by the time between the rising and falling edge of either pulse as shown in figure 4.1. The measured output can be seen to match the theoretical calculation of $4\mu s$.

The two distinct pulses are a result of the phase shift between the PHY crs_dv and the delayed crs_dv line. Additionally, the distance between the two pulses indicates the size of the packet.

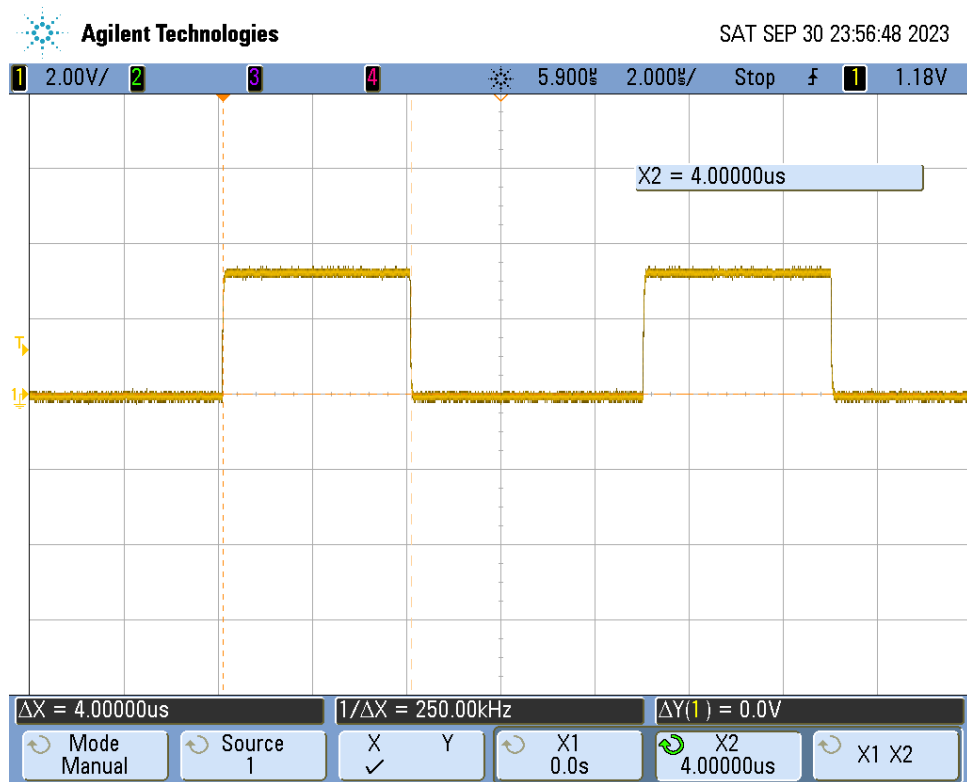


Figure 4.1: Added latency by packet filter waveform.

4.1.3 Improvements

A potential improvement on the design could be to integrate the packet classifier with the Ethernet MAC. This could reduce the added latency to zero by removing the need to store the packet in the additional shift register. The approach would involve storing the incoming packet and if the packet is later deemed to be blocked, the controlling FSM could be reset to ignore the packet.

4.2 Utilisation

Resource utilisation is an integral part in validating the feasibility of implementing the design on a particular FPGA or microchip. This section details the post synthesis resource utilisation of the design on the Nexys A7-100T FPGA using Xilinx Vivado 2022.2. Namely, the NEORV32, Ethernet hardware and packet filter are analysed.

The resource breakdown referred to in this section can be found in figure 4.2 while a more detailed breakdown of the resource utilisation including the primitives can be found in appendix A.2.

The design as a whole uses a total of 64.5% of the available slice LUTs, 12.9% of the available flip flops and 96.3% of the available BRAM.

4.2.1 NEORV32 processor

significant LUT usage was attributed to the 32-bit wide wishbone interface. Considerable LUT consumption relates to frame buffers used in Ethernet hardware, elucidated further in subsection 4.2.2.

Name	Slice LUTs	Slice Registers (126800)	F7 Muxes (31700)	F8 Muxes (15850)	Block RAM Tile (135)	DSPs (240)	Bonded IOB (210)	BUFGCTRL (32)	MMCME2_ADV (6)
↳ N hardware_top	40920	16457	2436	884	130	4	66	8	1
> ↳ neorv32_top_inst (neorv32_top)	28455	2507	25	8	130	4	0	0	0
↳ I ethernet_mac (wb_ethernet)	11738	12505	2403	872	0	0	0	0	0
↳ I eth_tx (eth_tx_mac)	9175	12384	2296	848	0	0	0	0	0
↳ I FCS_CRC32 (CRC)	49	40	0	0	0	0	0	0	0
↳ I eth_rx (eth_rx_mac)	1398	73	51	0	0	0	0	0	0
↳ I rmii_int (rmii)	1165	48	56	24	0	0	0	0	0
↳ I pc (packet_classifier)	571	1145	0	0	0	0	0	0	0
↳ I pf_stats_spi (pf_stats)	127	104	8	4	0	0	0	0	0
> ↳ clk_control (clk_master)	1	0	0	0	0	0	0	6	1

Figure 4.2: Summary of the resource utilisation on XC7A100T FPGA.

The NEORV32 SoC consumed the majority (69.5%, or 28455), of the slice LUTs in the design. While many interfaces were enabled such as SPI, UART, GPIO, external interupts (XIRQ) and the true random number generator, a considerable amount of the LUTs were consumed by the 32bit wide wishbone interface. More specifically, 25992 slice LUTs, or 91.3% of the NEORV32 usage.

The large LUT utilisation relates to the frame buffers used in the Ethernet hardware, elucidated further in section 4.2.2.

DSP48 blocks were also used by the SoC to handle the multiply operations to free up LUTs.

The instruction memory (IMEM) and data memory (DMEM) sizes were configured to optimise the remaining BRAM blocks for increasing flexibility in firmware. Specifically, IMEM was allocated 256KB while the DMEM (acting as RAM) amounting to 168KB.

4.2.2 Ethernet hardware

Comparatively, the Ethernet hardware accounted for 11738 slice LUTs and 12505 slice registers, most of which is consumed by the transmit logic (78% LUT and 99% registers). The considerable LUT utilisation in the transmit logic and NEORV32 Wishbone interface is due to the manner in which the frame buffer is written to. The complex operations such as address validation and array modification for writing to the frame buffer can be seen in listing 4.1. Notably, the address validation specifically implements a 32bit wide comparator and the need to write/modify to the frame buffer array causes large LUT utilisation.

```

1 if wb_i_addr >= x"13371004" and wb_i_addr <= x"13376410" then
2   -- Subtract 4100 from the address to get the virtual address
3   virtAddr := to_integer((unsigned(wb_i_addr(15 downto 0)) - 4100));
4   FRAME_BUFFER(8 + virtAddr) := wb_i_dat(31 downto 24);
5   FRAME_BUFFER(9 + virtAddr) := wb_i_dat(23 downto 16);
6   FRAME_BUFFER(10 + virtAddr) := wb_i_dat(15 downto 8);
7   FRAME_BUFFER(11 + virtAddr) := wb_i_dat(7 downto 0);
8 end if;

```

Listing 4.1: Code for writing to the frame buffer

This design choice also influenced the critical path delay as detailed further in section 4.3. Optimisations to this area would be imperative to drastically reduce the resource consumption and improve the critical path delay.

By contrast, the receive logic consumed far less resources of 12% of the Ethernet MAC’s LUTs and only 1% of the registers. This is attributed to the simpler design which stores the incoming packets with the correct endianness in the frame buffer before subsequently triggering an interrupt upon the packet’s arrival.

The rmii_init logic acts as the glue logic between the PHY and the MAC. It facilitates the clock and bus domain crossings between the 8bit wide 80Mhz MAC and the 2bit wide 50Mhz RMII PHY.

4.2.3 Packet filter

The packet classifier consumed a total of 571 slice LUTs and 1145 slice registers, suggesting a potential to increase the number of rules. Though, the fan-in and fan-out will likely need to be considered due to the nature of the implementation. The synthesiser’s decision to use registers over BRAM for rule storage is likely due to the rules being small in size and that the BRAM blocks are better used elsewhere.

Alternatively, the minimal resource utilisation indicates that the design is suitable for implementation on smaller FPGAs or ASIC designs and will have negligible impact on the overall silicon area.

4.3 Timing Summary

Timing analysis of the design provides insight into the critical path delay and the maximum frequency of the design. Basic results are presented in this section and are primarily around the Wishbone interface due to its role in the critical path. Importantly, the Wishbone interface operates at the same clock frequency as the NEORV32 processor which directly impacts the speed of the CPU for software based operations.

Initially, a single 50Mhz clock sourced from the onboard MMCM was used. A post-synthesis analysis indicated a positive slack in the design, allowing for the clock frequency to be updated to 80Mhz. This was done to increase the performance of the CPU so that it could process network packets faster in software.

After resynthesising, a worst negative slack for setup time of -2.634ns was reported with a total of 82 endpoints failing the constraints. Additionally, a worst hold slack of -0.021ns was reported. The identified critical path originates from the Wishbone interface to the BRAM block within the Ethernet hardware, shown in figure 4.3. Due to the NEORV32’s implementation of the Wishbone bus, the critical path cannot be easily improved and is the leading limitation in the speed of the design.

While in practice these timing constraints do not crucially impact the design’s operation, caution is advised in future adaptations or usage. Other paths were also encroaching on a slack of zero and hence

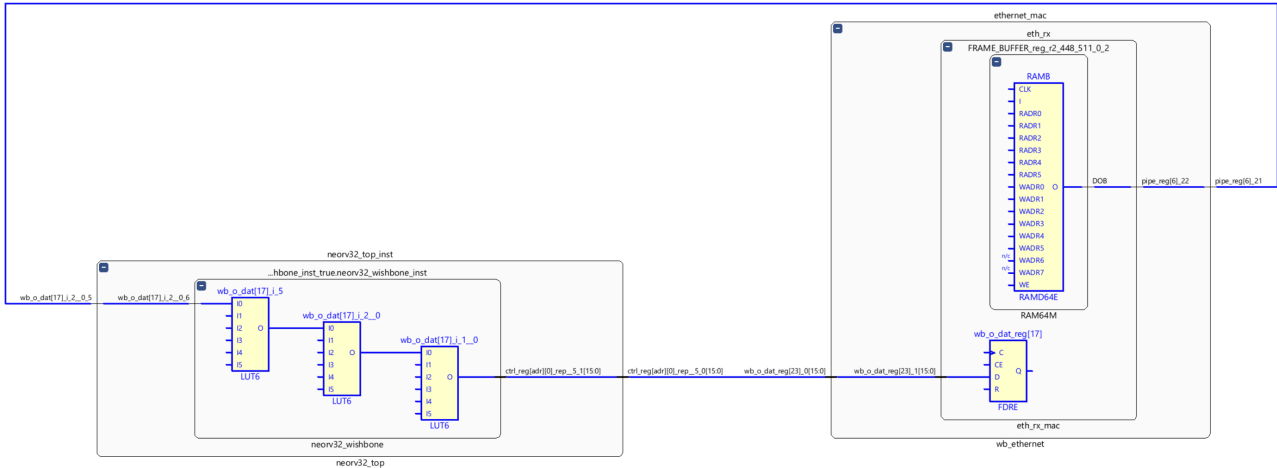


Figure 4.3: Critical path in SoC design.

the design was limited to 80Mhz. Testing at 90Mhz was conducted, however, the design was found to be unstable and had a large increase in the number of failing endpoints.

More accurate timing constraints would need to be set to acquire the absolute maximum frequency of the design. Though, this was outside the scope of this thesis.

4.4 Filtering performance

Blocking unwanted packets is imperative to a firewall's operation with any packets bypassing the filter rendering it useless. Testing all possible permutations of bits going through the firewall is infeasible due to the sheer number of packets needed, which is on the order of 2^{104} . For example, a complete testing suite for all source IP addresses alone would require 2^{32} (about 4.3 billion) packets to be sent to the device. Therefore, a small sample of packets, shown in table 4.1, were tested to ensure the filter is working as intended.

4.4.1 Test setup

Four hosts distributed across two networks were used to test the device as depicted in the network diagram in figure 4.4. The network consisted of three Raspberry Pi 4s and an x86 based Ubuntu machine. The specifics characteristics of these devices are irrelevant to this thesis, given that they all adhere to the TCP/IP standards. More specifically they were chosen due to their capability to run python scripts and are accessibility over Ethernet. A common script¹ was used on all devices to test each of the services available on different ports and protocols.

The rules shown in table 4.1 shows the rules that were loaded on the packet filter. While these test cases is only a subset of the total coverage, a mix of different combinations of ports, protocols and IP addresses were chosen. More specifically the rules were chosen to test the following cases:

- All devices can access the device in some way (eg, over ICMP),

¹The python *test* script can be found at <https://github.com/matty0005/thesis-tools>

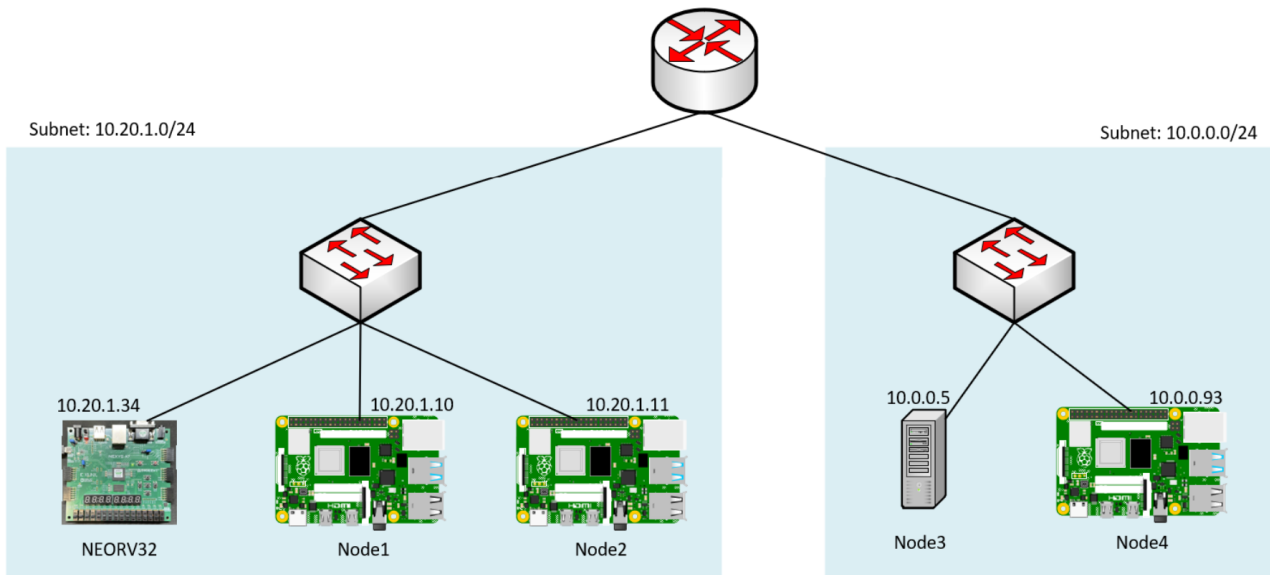


Figure 4.4: Network architecture for firewall tests.

- All machines could access at least two services,
- Identical ports over different protocols can be filtered (eg, port 1337 over TCP and UDP),
- Ports can be blocked on a device even though the device can access other services with the same protocol,
- The wildcard operator works in each field, and
- Any port that is not explicitly allowed is blocked.

By default, as the packet filter is a default-deny, any packet that doesn't fit these constraints is blocked and can be verified in the tests summarised in 4.2.

Table 4.1: Firewall configuration for testing

Source IP	Destination IP	Source Port	Destination Port	Protocol
any	10.20.1.34	n/a	n/a	ICMP
10.0.0.5	10.20.1.34	any	any	UDP
10.0.0.5	10.20.1.34	any	80	TCP
10.0.0.93	10.20.1.34	any	1337	TCP
10.0.0.93	10.20.1.34	any	9999	UDP
10.20.1.10	10.20.1.34	any	1337	any
10.20.1.10	10.20.1.34	any	any	UDP
10.20.1.11	10.20.1.34	any	9999	UDP

Typically, firewalls have a second interface that connects to a local network, allowing packets from multiple IP addresses to be processed and forwarded on. However, in this setup, a single device is behind the firewall, requiring the *destination IP*'s to be the same (the NEORV32's IP address, 10.20.1.34).

Additionally, the *source port* was configured to allow any source port through. This is important due to the client arbitrarily choosing the source port at random. Therefore, a wildcard was used as this makes the source port impossible to predict. It's worth noting that some niche programs operate with predictable ports, though none of the programs used in this test were of this nature.

4.4.2 Test results

A summary of the results can be seen in table 4.2 which show the firewall blocking and allowing the respective packets correctly.

Table 4.2: Summary of packets including expected and actual outcomes

Device	Dest. IP	Protocol	Src. Port	Dest. Port	Expected Outcome	Actual Outcome
Node1 (10.20.1.10)	10.20.1.34	TCP	Any	1337	Allow	Allowed
Node2 (10.20.1.11)	10.20.1.34	ICMP	-	-	Allow	Allowed
Node3 (10.0.0.5)	10.20.1.34	UDP	Any	9999	Allow	Allowed
Node4 (10.0.0.93)	10.20.1.34	TCP	Any	1337	Allow	Allowed
Node1 (10.20.1.10)	10.20.1.34	UDP	Any	1337	Allow	Allowed
Node3 (10.0.0.5)	10.20.1.34	TCP	Any	80	Allow	Allowed
Node3 (10.0.0.5)	10.20.1.34	TCP	Any	1337	Deny	Denied
Node2 (10.20.1.11)	10.20.1.34	TCP	Any	1337	Deny	Denied
Node4 (10.0.0.93)	10.20.1.34	UDP	Any	1337	Deny	Denied
Node4 (10.0.0.93)	10.20.1.34	TCP	Any	80	Deny	Denied

The detailed output from the script on each host is available in appendix A.7. While these tests don't formally prove the firewall is correctly working, they do provide substantial evidence of the design's correctness. It's important to note that additional rigorous testing, which wasn't formally documented, was conducted throughout the development of the design. Such an example test case involves spamming ping packets from one host while sending valid packets from another.

These results stipulate the devices suitability for use in a real world environment. The filter exhibits capacity to filter out the significant majority of unwanted packets, making it ideal for low security applications. However, formal verification and meticulous testing is imperative to suitability for high-security applications. With the absence of these in the above tests, the design would necessitate further validation to be deployed in high security environments.

4.5 Comparison to preexisting solutions

To ensure the effectiveness of the designed hardware, comparisons to preexisting solutions with *Fast Ethernet* (100Mbits/s) were conducted. The selected devices include the WIZ5500 Pico¹, Nucleo-F767ZI² and MilkV-Duo³.

The WIZ5500 Pico integrates a *Raspberry Pi RP2040* (ARM-based) as its MCU, operating at 133Mhz, and employs the *WIZ5500* IC to manage Ethernet traffic. Notably, the WIZ5500 handles layers one to four onboard and interfaces over SPI. This is in contrast to the other designs compared which use an external PHY and then have the higher layers in software.

The Nucleo-F767ZI (referred to as just F767ZI) is powered by the *STM32F767* (ARM-based) MCU and features an onboard *LAN8742A* PHY chip. Similarly to the Nexys A7 board, the LAN8742A PHY chip connects to the STM32F767 over RMII and has hardware support for. This establishes a good comparison between the two devices from a hardware perspective. However, unlike the Nexys A7, it utilised the LwIP network stack opposed to FreeRTOS-Plus-TCP.

The most contemporary board in the lineup is the MilkV-Duo which employs the 64-bit RISC-V *CVITEK CV1800B* processor. Operating at 1Ghz, the dual-core processor includes 64MB of RAM and incorporates an Ethernet MAC and PHY directly within the same package. The MilkV runs vanilla Linux on the first core and FreeRTOS on the second. Throughout these tests, Linux was used as it had greater support at the time of testing.

The following sections detail the relative performance of the respective devices in terms of latency, throughput, security and power consumption. Thermal measurements are also conducted to bring greater detail to the power consumption of the devices.

4.5.1 Network latency tests

A simply UDP ping program was devised on each device to empirically assess the round-trip-time (RTT). This not only helps understand the latency of the system as a while, but by using two different packet sizes, the software overhead can be assessed. The program was configured to receive a UDP packet on port 9999 and reply with a corresponding packet.

¹See: <https://www.wiznet.io/product-item/w5500-evb-pico/>

²See: <https://www.st.com/en/evaluation-tools/nucleo-f767zi.html>

³See: <https://milkv.io/duo>

To alleviate nuances in the network and once off delays, 1,000 UDP packets were averaged and the results are presented in 4.5. A table highlighting the numerical values of the results can be found in appendix A.4.

Two specific UDP payloads sizes, 8 bytes and 256 bytes, were selected to evaluate the software overhead.

These values were chosen due to the additional time required to process the packet in hardware is in the order of nanoseconds. More specifically, the delay can be calculated by knowing the bitrate and difference in packet size. In this test, at a speed of 100Mbit/s, sending 248 more bytes takes an additional $\frac{248 \times 8}{100 \times 10^6} = 19.84\mu s$. In contrast, software processing time scales up significantly with the packet size, due to additional data manipulation and processing

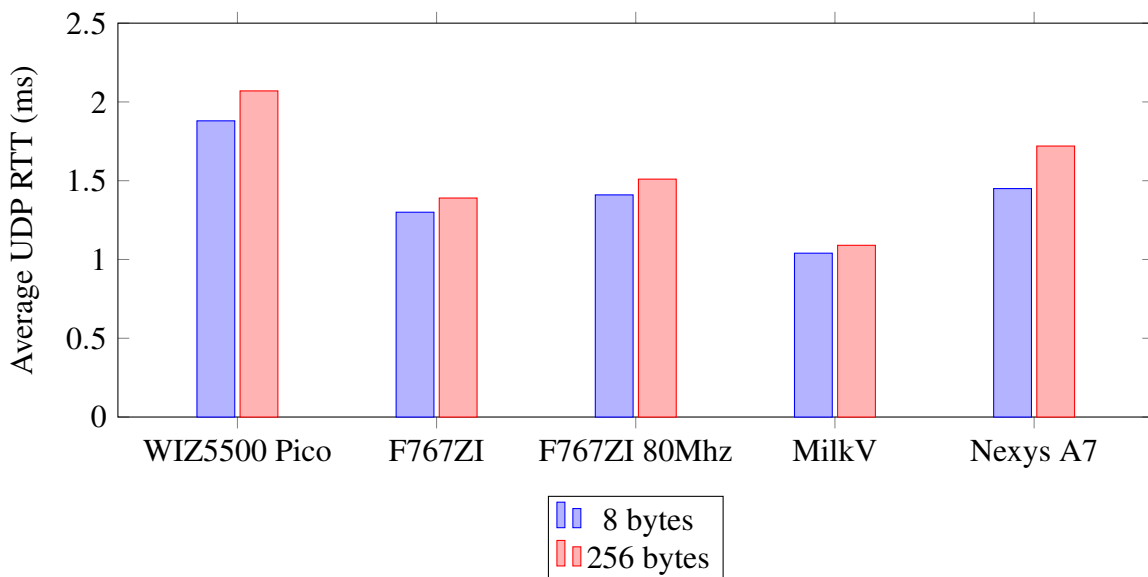


Figure 4.5: Average UDP RTT for different devices and payload sizes.

Testing on the Nexys A7 resulted a larger difference compared to the competing products and indicates a larger software overhead. It is hypothesised that this is a consequence if the FreeRTOS-Plus-TCP stack, which likely requires more computations per packet than LwIP on the F767ZI. Two tests on the F767ZI was conducted to understand the effect of clock frequency, one at the default 96Mhz and another at 80Mhz to match the Nexys A7. The results indicated a small improvement in latency of 0.11ms when using 96Mhz clock speed on the F767ZI. A decrease in latency is expected on the Nexys A7 if the clock frequency can be increased. This is further supported with the MilkV Duo which runs at 1Ghz and has a lower latency than both the F767ZI and Nexys A7.

The results from this section support the design given in this thesis is comparable to preexisting solutions in terms of overall latency. However, latency is not the only metric used in assessing network performance. Network throughput is another imperative metric and is discussed in the next section.

4.5.2 Network throughput tests

This section primarily focuses on the throughput tests amount the F767ZI, MilkV Duo and Nexys A7 boards. The WIZ5500 Pico was exempt from testing due to a lack of support for Iperf 3, a universally

accepted tool for bandwidth testing between two devices. Both FreeRTOS and LwIP have Iperf 3 server implementations which were used to test the throughput of the devices.

The client device, an x86-based desktop machine, was connected to the network at gigabit speeds, ensuring there was no bottleneck on the client side. Test results were averaged over ten runs to ensure accuracy and account for any anomalies. Table 4.3 summaries the bitrates of the tested devices. The detailed Iperf 3 outputs from each test can be found in appendix A.8.

Table 4.3: Bitrate of various embedded devices

Device	Bitrate
Nexys A7	1.32Mbits/s
F767ZI	7.11Mbits/s
MilkV	92.4Mbits/s

The MilkV Duo with the 1Ghz processor, saturated the 100Mbit/s *Fast Ethernet* interface, aligning with expectations. The test is consistent with the hypothesis that software constraints bottleneck the Nexys A7's performance. It is also believed that suboptimal task priorities and interrupt configurations in FreeRTOS are contributing to this limitation, as demonstrated by the dip in performance when the tick frequency in FreeRTOS was altered from 500Hz to 1000Hz, causing a notable 41.8% reduction in performance. This would make the scheduler interrupt the tasks more frequently and hence give less time for the packet to be processed before switching tasks.

The F767ZI showcased a superior throughput over the Nexys A7, attributed primarily to the utilisation of LwIP over FreeRTOS-Plus-TCP and having more refined drivers with better interrupt handling and task scheduling.

While the Nexys A7 provides comparable performance in the UDP ping tests, the throughput is lacking and provides an opportunity for improvement in the firmware. Despite this, the Nexys A7, which employs a hardware firewall, holds an advantage in terms of security, which is discussed in the next section.

4.5.3 Security analysis

The distinctive feature of the design on the Nexys A7, developed in this thesis, is the incorporation of a hardware packet filter, whereas the other devices rely on software-based packet filters. This hardware approach benefits from intrinsic robustness against particular vulnerabilities typically found within embedded systems, such as power-glitch attacks (also commonly referred to as fault-injection).

Power-glitch attacks, while hard to execute in a real world situation, provide a threat to embedded systems, characterised by rapid power off-and-on cycles at critical sections aimed at bypassing specific code instructions. Although in practice, these attacks are extremely rare, it does provide an advantage to the hardware firewall in system security and robustness.

The design in this thesis operates by directly interfacing and processing the bits with the PHY which makes it less susceptible to power-glitch attacks. This is due to comparison logic being independent of

the CPU and not consisting of a set of instructions, but rather a set of dedicated logic which is more resilient. Furthermore, the attack surface (a group of potential vulnerabilities accessible to a malicious actor) of the design is much smaller due to much fewer known hardware vulnerabilities. It is worth noting that exhaustive formal verification would be necessary to ensure the design is secure against power-glitch attacks. However, this was outside the scope of this thesis.

As discussed earlier in this thesis, a benefit of hardware packet filters is the latency performance. Consequently, the firewall latency was compared with preexisting software solutions in the next section.

4.5.4 Firewall latency

To accurately gauge the latency introduced by software firewalls, a GPIO pin was configured to toggle states, marking the entry and exit of a packet during the filtering process. This approach makes the assumption that the latency involved in setting the GPIO pin states is reciprocal and the turn on and turn off time is the same, thereby minimising the potential influence on the overall delay measurement.

For consistency and to ensure a level playing field in the comparisons, the software based implementation of the firewall on the Nucleo-F767ZI board used eight rules. This aligns with the FPGA design's limitation and ensures the analysis remains fair.

Utilising an oscilloscope enabled precise time measurements of the firewall latency as found in figure 4.6. These measurements revealed the timings are dependent on the quantity and the positioning of the applied rules. For example, the best case scenario is when the first rule is matched, resulting in a lower latency, whereas the worst case is when the last rule is matched, resulting in a higher latency.

A best case time was measured to be $3.14\mu s$ (figure 4.6a) while an average case was $10.76\mu s$ (figure 4.6b).



Figure 4.6: Software packet classifier timings

The lower latency observed in the ideal software scenario (figure 4.6a) is attributed to the packet matching the first rule, thereby reducing the necessary computations. This made the software filter quicker than the hardware filter in this case. However, in real-world applications, it is impractical to

assume that the first rule will always be matched. Instead, the average-case latency is more indicative of actual performance.

It is important to recognise that these delays influence throughput as the processor is limited to only one task at a time and cannot multitask.

In low bandwidth environments, there is little benefit, excluding their security advantage, to hardware firewalls in embedded systems. However, in scenarios where latency holds a significance, such as real-time robotic control systems, or where utmost security is imperative, as seen in secure access control systems, hardware firewalls provide as a more superior solution. Another difference between hardware and software implementations is the efficiency of the design, which will be detailed in the next section.

4.5.5 Power consumed between boards

This section considers the power consumed between the four boards compared in this chapter. Detailed power analysis on the Nexys A7 board can be found in section 4.6. The *Nordic Semiconductor Power Profiler Kit 2* (PPK2) was used to measure the current consumption of the device over time. As all systems in these tests operate at 5V, only the current will be measured. A summary of the results can be found in figure 4.7, while the data in tabular form can be found in appendix A.5.

Each board underwent four different tests to measure current consumption: Idle, Busy, No Ethernet, and Clean State. In the *Idle* measurement, the design is loaded but not processing any packets or computing anything. For the *Busy* test, measurements were taken while the device actively received and processed packets. It should be noted that these values are typically lower than the Idle measurements, as the flashing status LED tends to impact the power consumption more than the hardware's power consumption. The *No Ethernet* test refers to measurements taken when the device is idle with the Ethernet cable disconnected, showcasing the PHY chips' low-power sleep-like state in the absence of an Ethernet connection. Lastly, the *Clean State* involves measuring the device while idling with no design loaded, effectively measuring the quiescent current of the device.

Analysing figure 4.7 reveals the differences between the clean and busy states. The Nexys A7 board displayed the largest discrepancy, with a 99.27mA difference, compared to the 87.94mA difference observed in the F767ZI board. It's worth noting that the Nexys A7's clean state measurement was taken without the hardware design applied (Ethernet MAC, packet filter, and RISC-V core), resulting in a separate reading of 283.75mA when the design and hardware was loaded (excluding firmware). This indicates that, despite having the highest quiescent current, the Nexys A7 also exhibits the largest design current for the project. Power optimisations would be necessary in components such as the Ethernet and the RISC-V core to perform closer to preexisting solutions, although this was not a primary focus of this thesis.

All these tests were conducted without enabling a firewall. Additional tests were carried out to assess the Nexys A7 board's current consumption with the hardware firewall enabled and with a software firewall implemented on the F767ZI. No measurable differences were observed when the

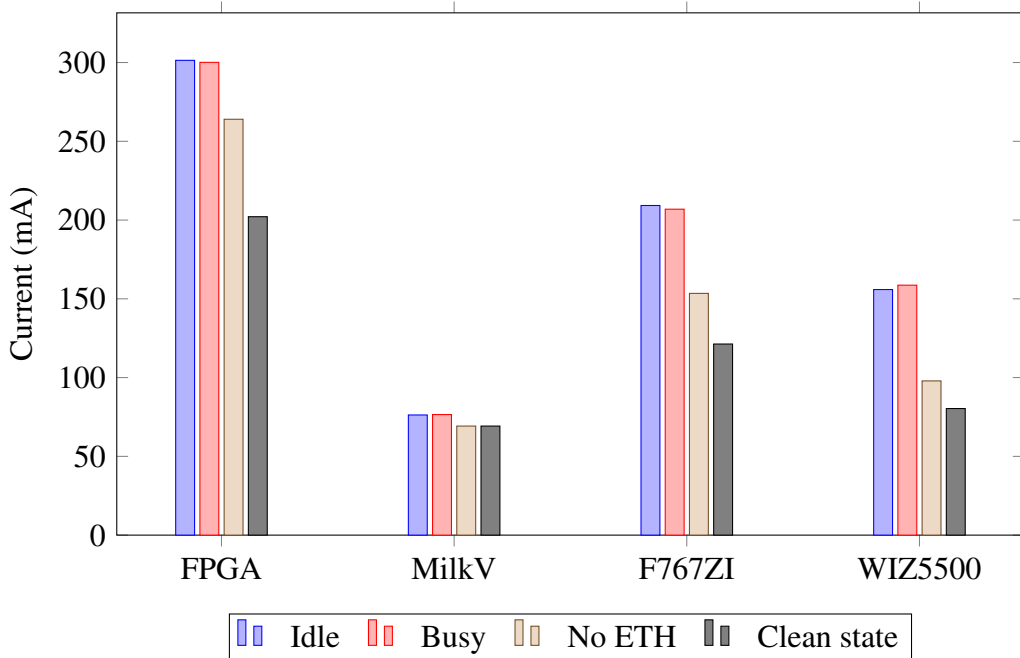


Figure 4.7: Comparison of Idle, Busy, and No eth currents for devices

hardware packet filter was enabled or disabled, possibly attributed to the limited resolution of the measurement equipment. However, the software implementation resulted in a relative increase of 1mA due to the execution of more comparisons per packet.

Currently, the outcomes suggest that the Nexys A7 board might not be ideal for low-power applications due to its considerable quiescent current. The board is primarily intended for developmental purposes and not for power efficiency. In a production setting, a revised board design would omit unnecessary components and could incorporate more energy-efficient designs or FPGAs. While this falls outside the scope for this thesis, it is an important consideration for future work.

Moreover, current consumption naturally correlates with heat production of the device. By using a thermal camera, one can learn where the majority of the power is being drawn and as such is discussed in the next section.

4.5.6 Thermal analysis

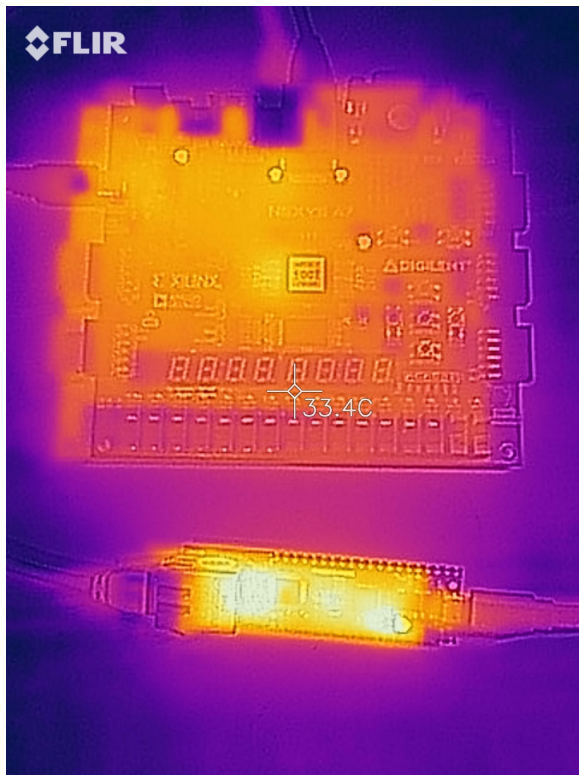
A Flir One thermal camera was used to periodically record the temperatures of the boards and a summary of results is provided in table 4.4. Throughout the examination, a constant ambient room temperature of 24.8°C was maintained. Measurements were taken at 5, 10, 30, 60 and 120 minute intervals to track the influence of the PCB board had on the thermal properties of the chips. This consideration is important as larger PCBs possess greater thermal mass which can distort the results and require time to get up-to temperature. Detailed results can be found in appendix A.6. Since no substantial thermal variations were observed after 60 minutes, the tests was concluded at the 120-minute mark.

Refer to figure 4.8 for a visual representation of each board's thermal distribution after two hours. It's important to consider these measurements as indicative rather than conclusive, highlighting the

Table 4.4: Temperature comparison of different chips during the test

Time	Chip	Temperature (°C)
5 min	WIZ5500	58.0
	FPGA	38.0
	MilkV	36.7
	F767ZI	35.9
2 hours	WIZ5500	56.8
	FPGA	40.4
	MilkV	38.1
	F767ZI	36.8

chips' relative temperatures and hotspots. This is because discrepancies are expected due to the thermal camera's self-calibration process and the manual aiming of the camera to capture maximum heat being inherently inaccurate.



(a) Nexys A7 (top) and WIZ5500 Pico (bottom)



(b) Nucleo board (left) and MilkV Duo (right)

Figure 4.8: Thermal images of boards under test after two hours

From figure 4.8a, the Nexys A7 exhibits additional hotspots besides the FPGA itself, likely indicating that other components are contributing to the elevated quiescent current noted earlier. When compared with other designs, the Nexys A7 FPGA shows minimal heat output, indicating a more efficient design. However, it is important to consider the physical dimensions of the chips and their respective thermal masses.

Among the evaluated boards, the WIZ5500 exhibited the highest temperature, while the MilkV board demonstrated the lowest heat emission. The larger F767ZI board displayed a comparatively

lower temperature despite having a much larger footprint and an extra PHY chip contributing to its overall heat output. In contrast, the MilkV incorporates an MCU, Ethernet MAC, and PHY within the same package. These observations indicate that WIZ5500 may not be the optimal choice for thermally sensitive applications such as recording room temperatures. Alternatives like the MilkV or an FPGA on a more efficient board with a design similar to the one created in this thesis may be more suitable.

Although these thermal measurements do not provide a great deal of useful information, they help indicate that the Nexys A7's significant power draw is not predominantly attributed to the FPGA itself and instead showcases the device's relative efficiency. The following section delves deeper into the power consumption of the design.

4.6 Power analysis

4.6.1 Theoretical power analysis

In this section, the power consumption of the design is analysed theoretically using Xilinx Vivado's post-synthesis power analysis summary. The findings from this summary provide useful insights into the design. However, it is important to note that these results are dependent on many variables and should only be considered as an indication of the design's power consumption.

The design's total power consumption was calculated to be 487mW, as shown in figure 4.9. A large portion of this, 383mW, is attributed to dynamic power, which fluctuates depending on the current state and operations of the design.

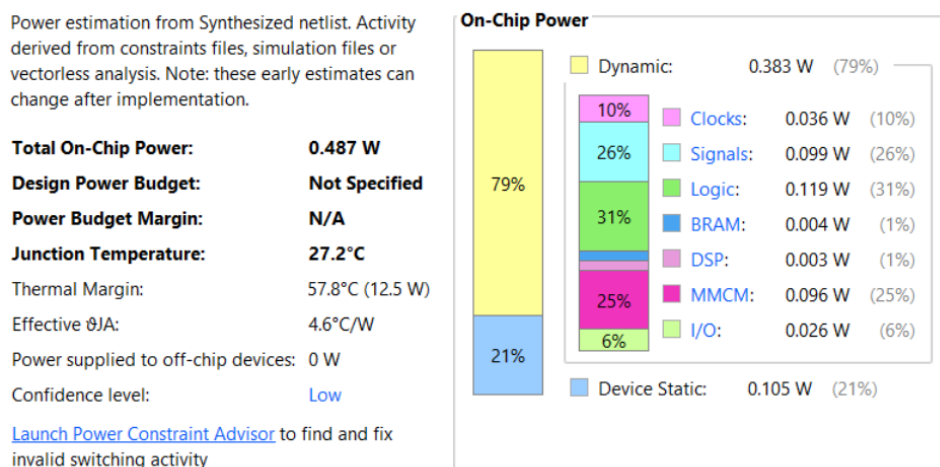


Figure 4.9: Post synthesis power summary for design.

Vivado further breaks down the design's power consumption into the different hierarchical components, as shown in table A.5. Notably, the RISC-V processor (NEORV32) constitutes to the majority of the power consumption in the design. In contrast, the Ethernet hardware consumes under 100mW while the packet classifier consumes just 2mW. This implies that incorporating a packet classifier into a design comes at a minimal power cost, making it ideal to be included in low power systems.

Table 4.5: Power consumption of components.

Name	Total (mW)
neorv32	158
clk control	97
ethernet_mac	97
packet classifier	2

4.6.2 Measured power analysis

For the empirical analysis, the current was measured since the voltage remained constant across devices (5V from USB power). The Nordic Semiconductor PPK2, used for current measurements, can record up to 100kSa/s. However, a 10kSa/s sampling rate was chosen to reduce noise in the results. It's important to treat these results as indication of power consumption as they do not account for regulator inefficiencies and do not give a true power rating of the core parts of the design.

As a baseline, the Nexys A7 board with no design loaded drew 200mA (1W at 5V), which is attributable to all the board's additional components. Upon loading the hardware design (not including the firmware), the current consumption increased to 284.4mA. After flashing the firmware, the idle current reached an average of 301.84mA, or a power draw of 1.51W was observed. Deducting the quiescent current of the board's miscellaneous components (assumed to be the baseline 200mA measurement) yields a power consumption of 0.51W, roughly aligning with the synthesis tool's calculations.

A series of tests were conducted including sending ICMP pings and web requests. When the device was pinged at 50ms intervals, the average current of 300.72mA was measured. Interestingly, the current consumption patterns were cyclic in nature, as illustrated in figure 4.10. Subsequent UDP ping tests resulted in a similar waveform pattern, with an average current draw of 301.13mA.

This phenomenon was explored further by blocking the network packets using the packet filter. The results revealed that the filter had a negligible impact on the current consumption, with an average current of 300.92mA. Notably, the cycle's periodicity, approximately 83ms which not only exceeds to the 50ms time between pings, but is also consistent with the previous tests, indicating that it's not a consequence of the firmware. Secondary observations were made by capturing the PHY status LED at 240 frames per second which revealed a 20-frame period (approximately 84ms), consistent with the current measurements indicating that the difference in current is due to the LED.

The subsequent test was centred around accessing the webserver, and the results are detailed in figure 4.11, where five distinctive regions are depicted, each corresponding to a specific action.

The first action (on the far left) is the initial HTTP GET requests. Notably, this section is split in two, as the client fetches the html, css, and favicon first, followed by a request for a considerably larger javascript file. The readings for each of these points are given as: average current, maximum current, and time, going from top to bottom.

The second section was triggered by navigating to the 'about page'. The third part of the test involves navigating to the config page, while the fourth segment is initiated by pressing the 'load rules'

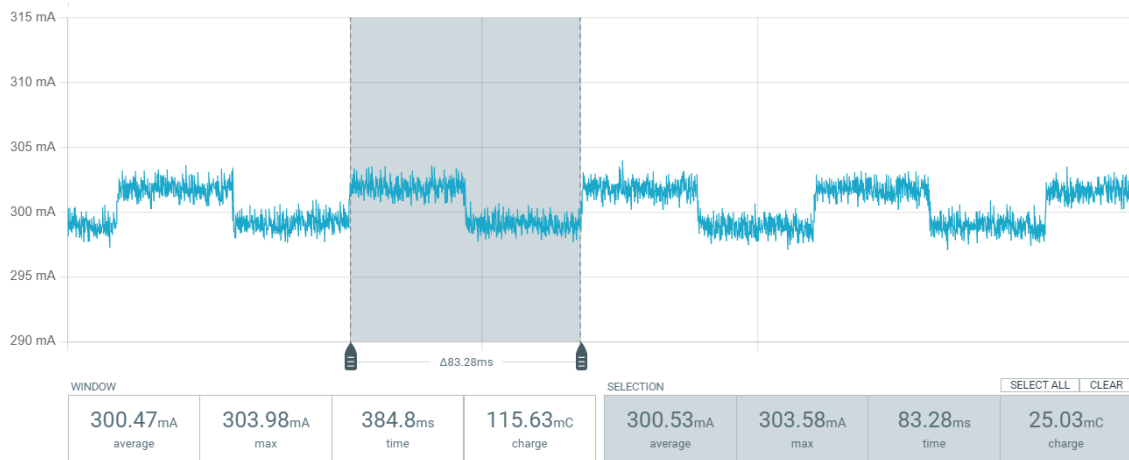


Figure 4.10: Zoomed in current consumption for ICMP pings.

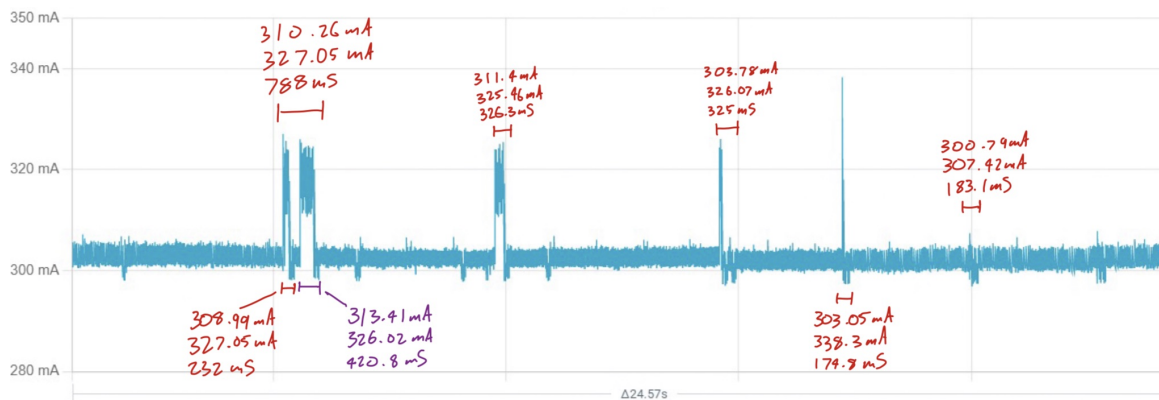


Figure 4.11: Current consumption of Nexys A7 with HTTP requests.

button on the config page. The final test case is a result of refreshing the statistics on the main page.

A crucial observation to highlight is the role of client side routing and rendering, which makes subsequent full-page requests unnecessary and instead, only requires smaller API requests for data updates. The savings are two-fold due to the reduced network traffic and not requiring and SD card read or write operations, which greatly impact the current consumption. The fourth request, albeit involving an SD card read, is limited to accessing a single page due to the small file it is accessing. Conversely, the fifth request does not include SD card read/write operations, instead only a single SPI transaction, which consequently consumes significantly less power.

An essential learning from this is the efficacy of static page applications with client-side routing, like those created with Vue.js, in embedded systems for minimising resource utilisation, network traffic and power consumption. Another result from these tests is the negligible impact of the packet filter on the power consumption, which is Vivado predicted, making it a perfect addition to future microprocessors with built-in Ethernet MACs.

Chapter 5

Conclusion

5.1 Limitations

While this thesis explored the design and implementation of a hardware packet filter, Ethernet MAC with a RISC-V softcore processor, there are some limitations to the design and the research conducted. These can be summarised in the following points:

- The current system only supports filtering network packets in one direction as it assumes all packets leaving the device is safe.
- The design only considers IPv4 packets without IEEE 802.1Q VLAN tagging.
- The transmit logic is not optimised for resource usage and can be improved.
- Only one interface is supported due to the bandwidth limitations of the PMOD ports on the Nexys A7 board.
- Only HTTP and other unencrypted protocols are supported.
- The current design is bottlenecked from the processor - NEORV32

In addition, only one interface is supported due to the Nexys A7 board only consisting of one ethernet PHY and the additional PMOD ports are not suitable for Ethernet. This is because the PMOD ports are only rated for a 25Mhz bandwidth, while the RMII signals are 50Mhz. As such, signal integrity issues arose (see appendix A.9 for eye diagram) and restricted the use to just one interface - the onboard PHY. A new development board with two PHYs would be needed.

5.2 Sustainability

Ethernet standards have been in place since 1985 [26] and the IP, TCP, UDP and other layer 4 protocols have been in service for decades and have not changed. Typically when new features are added in

these areas, they are added ontop of and not modify the packet structure itself. Such event was in 1998 with the introduction of IPv6 [39].

While malicious bad actors come up with new and innovative ways to breach a system, the core of this packet filter is solid and fundamentally should not need to change in future. Instead other additions and modification should be made to the system architecture to improve security, including but not limited to, HTTPS, public key cryptography and deep packet inspection.

Using the neorv32 while is feature-rich, as it's in its development process and new features are continually getting added and existing features moved around, it doesn't make for the best choice for ease of updating, but it does get regularly updated so if there was a security vulnerability, odds are that it will get patched.

Similarly, the FreeRTOS-Plus-TCP is a first-party library for FreeRTOS and is actively maintained. It is also feature-rich and is continually getting updated, however, its documentation and community support is more limited than that of LwIP.

Perhaps a larger issue with sustainability is the lifecycle of a Vue.js webapp. When updates are needed, potentially new versions of the toolchain may be needed thus contributing to longer development times.

Choice of riscv makes this project easy to commercialise since there is no licences needed for the risc-v cores are royalty free and the specific variant, neorv32 is open sourced under the BSD-3-Clause license.¹

This design was deployed on a Xilinx Artix 7 FPGA board with the LAN8720A PHY. As the LAN8720A chip uses the standardised RMII interface, there should be no issues porting the project to another FPGA or FPGA board so long as there is sufficient LUTs and BRAM available on the FPGA and uses an RMII phy. The hardware could be updated to RGMII or XGMII without too many issues with the main difference being in the input and output FIFO being able to support the different clock rates and bit widths.

5.3 Recommendations and future work

In light of the findings in this thesis, several key recommendations can be made for future work in the area of embedded system SoC design which features Ethernet connectivity.

The primary recommendation is to incorporate dedicated hardware packet filtering into SoC designs. As demonstrated in this thesis, the resource utilisation for the packet filtering logic is minimal (571 slice LUTs and 1145 slice registers) and can be easily integrated into the design with minimal impact to cost. Superior latency, throughput and power consumption metrics are only some of the benefits presented in this thesis over the conventional software based packet filters. Additionally, the potential resilience against potential security vulnerabilities is another key advantage of this approach.

While the NEORV32 is a solid general-purpose softcore processor, it seemed to bottleneck the design and withheld the design from achieving better performance. The CVITEK CV1800B, used in the

¹See: <https://github.com/stnolting/neorv32/blob/main/LICENSE>

MilkV-Duo and compared in this thesis, is a powerful SoC with an abundance of resources including a hardware MAC and PHY, but falls short of including a hardware packet filter. An ideal choice would be to have the performance of the CVITEK CV1800B with the hardware packet filtering capabilities of the design presented in this thesis. This would give the best of both worlds, performance and security.

Alternatively, research into using hybrid SoC FPGAs such as the Xilinx Zynq lineup which include an FPGA and a hardcore processor connected over a high speed fabric could be a good avenue. This provides the flexibility of an FPGA with the performance of a hardcore processor, ideal for small scale designs that would otherwise be too expensive for custom silicon.

Leveraging single page application frameworks such as Vue.js for use in embedded systems is another recommendation resulting from the work done in this thesis. Light-weight applications and low power devices can benefit greatly from the use of such frameworks as fewer network traffic is required due to client-side routing and static web content. In combination with a lightweight API, dynamic data can be obtained with minimal network traffic, making the user experience seamless and responsive.

In addition to these recommendations for future designs, the work in this thesis can be extended in the following areas:

- Redesign of the transmit logic to consume less resources while not losing on speed/performance,
- Add a second Ethernet interface to filter traffic for other devices on the network,
- Utilise the DDR2 RAM to free up BRAM in the FPGA,
- Implement public key cryptography for HTTPS,
- Support faster media interfaces, eg RGMII for 1Gbit/s or XGMII for 10Gbit/s,
- Use a different bus interconnect for the processor, eg AXI4, and
- Look into using LwIP over FreeRTOS-Plus-TCP.

5.4 Summary

This thesis explored the design and implementation of a hardware packet filter, Ethernet MAC with a RISC-V softcore processor. The design was implemented on a Xilinx Artix 7 FPGA board with the LAN8720A PHY. The design was able to achieve a throughput of 94Mbit/s with a latency of 1.04ms. The design was also able to achieve a power consumption of 128mA at 94Mbit/s.

Bibliography

- [1] S. J. Shapiro, “The strange story of the teens behind the mirai botnet,” Sep 2023.
- [2] A. C. S. Center, “Acsc annual cyber threat report, july 2021 to june 2022.” <https://www.cyber.gov.au/acsc/view-all-content/reports-and-statistics/acsc-annual-cyber-threat-report-july-2021-june-2022>, Nov 2022.
- [3] IHS, “The internet of things: a movement, not a market.” https://cdn.ihs.com/www/pdf/IoT_ebook.pdf, 2017.
- [4] W. Shi, G. Pallis, and Z. Xu, “Edge computing [scanning the issue],” *Proceedings of the IEEE*, vol. 107, no. 8, pp. 1474–1481, 2019.
- [5] M. Caprolu, R. Di Pietro, F. Lombardi, and S. Raponi, “Edge computing perspectives: Architectures, technologies, and open security issues,” in *2019 IEEE International Conference on Edge Computing (EDGE)*, pp. 116–123, IEEE, 2019.
- [6] E. D. Zwicky, S. Cooper, and D. B. Chapman, *Building Internet Firewalls (2nd Ed.)*. USA: O’Reilly and Associates, Inc., 2000.
- [7] E. W. Fulp, “Chapter e74 - firewalls,” in *Computer and Information Security Handbook*, pp. e219–e237, Elsevier Inc, third edition ed., 2017.
- [8] A. Wicaksana and A. Sasongko, “Fast and reconfigurable packet classification engine in fpga-based firewall,” in *Proceedings of the 2011 International Conference on Electrical Engineering and Informatics*, (Ithaca), pp. 1–6, IEEE, 2016.
- [9] S. Wasti, “Hardware assisted packet filtering firewall.” <https://madmuc.usask.ca/Pubs/shw320.pdf>, 2001.
- [10] S. M. Trimberger, “Three ages of fpgas: A retrospective on the first thirty years of fpga technology,” *Proceedings of the IEEE*, vol. 103, no. 3, pp. 318–331, 2015.
- [11] M. Gokhale and L. Shannon, “Fpga computing,” *IEEE MICRO*, vol. 41, no. 4, pp. 6–7, 2021.

- [12] S. Lin, D. Zhang, Y. Fu, and S. Wang, “A design of the ethernet firewall based on fpga,” in *2017 10th International Congress on Image and Signal Processing, BioMedical Engineering and Informatics (CISP-BMEI)*, vol. 2018-, pp. 1–5, IEEE, 2017.
- [13] A. Kayssi, L. Harik, R. Ferzli, and M. Fawaz, “Fpga-based internet protocol firewall chip,” in *ICECS 2000. 7th IEEE International Conference on Electronics, Circuits and Systems (Cat. No.00EX445)*, vol. 1, pp. 316–319 vol.1, IEEE, 2000.
- [14] S. M. Keni and S. Mande, “Packet filtering for ipv4 protocol using fpga,” in *2018 Second International Conference on Intelligent Computing and Control Systems (ICICCS)*, pp. 400–403, IEEE, 2018.
- [15] S. Cuenca-Asensi, A. Martínez-Álvarez, F. Restrepo-Calle, F. R. Palomo, H. Guzmán-Miranda, and M. A. Aguirre, “Soft core based embedded systems in critical aerospace applications,” *Journal of systems architecture*, vol. 57, no. 10, pp. 886–895, 2011.
- [16] L. Janik, M. Novak, L. Hudcova, O. Wilfert, and A. Dobesch, “Lwip based network solution for microblaze,” in *2016 International Conference on Broadband Communications for Next Generation Networks and Multimedia Applications (CoBCom)*, pp. 1–4, IEEE, 2016.
- [17] N. Joshi, P. Dakhole, and P. Zode, “Embedded web server on nios ii embedded fpga platform,” in *2009 Second International Conference on Emerging Trends in Engineering and Technology*, pp. 372–377, IEEE, 2009.
- [18] Y.-H. Cheng, L.-B. Huang, Y.-J. Cui, S. Ma, Y.-W. Wang, and B.-C. Sui, “Rv16: An ultra-low-cost embedded risc-v processor core,” *Journal of computer science and technology*, vol. 37, no. 6, pp. 1307–1319, 2022.
- [19] C. Heinz, Y. Lavan, J. Hofmann, and A. Koch, “A catalog and in-hardware evaluation of open-source drop-in compatible risc-v softcore processors,” in *2019 International Conference on ReConfigurable Computing and FPGAs (ReConFig)*, pp. 1–8, IEEE, 2019.
- [20] V. A. Frolov, V. A. Galaktionov, and V. V. Sanzharov, “Investigation of risc-v,” *Programming and computer software*, vol. 47, no. 7, pp. 493–504, 2021.
- [21] M. A. ISLAM and K. KISE, “An efficient resource shared risc-v multicore architecture,” *IEICE transactions on information and systems*, vol. E105.D, no. 9, pp. 1506–1515, 2022.
- [22] S. Nolting, “The neorv32 risc-v processor.” <https://stnolting.github.io/neorv32/>, 2023. v1.8.1-r17-gd1b295de.
- [23] “Wishbone B4 SoC Interconnection.” https://cdn.opencores.org/downloads/wbspec_b4.pdf, Dec. 2010. Standard.
- [24] W. Odom, *CCENT/CCNA ICND 1 100-105 Official Cert Guide*. Cisco Press, May 2016.

- [25] “Internet Protocol.” RFC 791, Sept. 1981.
- [26] “IEEE 802.3-2012 IEEE Standard for Ethernet,” standard, The Institute of Electrical and Electronics Engineers, Inc., New York, USA, Dec. 2012.
- [27] J. Hemanth, X. Fernando, P. Lafata, and Z. Baig, “An optimized packet transceiver design for ethernet-mac layer based on fpga,” in *International Conference on Intelligent Data Communication Technologies and Internet of Things (ICICI) 2018*, vol. 26 of *Lecture Notes on Data Engineering and Communications Technologies*, pp. 725–732, Switzerland: Springer International Publishing AG, 2019.
- [28] Microchip Technology Incorporated, “Small footprint rmii 10/100 ethernet transceiver with hp auto-mdix support.” "<https://ww1.microchip.com/downloads/en/DeviceDoc/8720a.pdf>", 2012. Revision 1.4 (08-23-12).
- [29] J. Sütő and S. Oniga, “Fpga implemented reduced ethernet mac,” in *2013 IEEE 4th International Conference on Cognitive Infocommunications (CogInfoCom)*, pp. 29–32, 2013.
- [30] J. Mitra and T. Nayak, “Reconfigurable very high throughput low latency vlsi (fpga) design architecture of crc 32,” *Integration (Amsterdam)*, vol. 56, pp. 1–14, 2017.
- [31] P. Guoteng, L. Li, O. Guodong, F. Qingchao, and B. Han, “Design and verification of a mac controller based on axi bus,” in *2013 Third International Conference on Intelligent System Design and Engineering Applications*, pp. 558–562, IEEE, 2013.
- [32] N. M. Khalilzad, F. Yekeh, L. Asplund, and M. Pordel, “Fpga implementation of real-time ethernet communication using rmii interface,” in *2011 IEEE 3rd International Conference on Communication Software and Networks*, pp. 35–39, IEEE, 2011.
- [33] T. Stuckenberg, M. Gottschlich, S. Nolting, and H. Blume, “Design and optimization of an arm cortex-m based soc for tcp/ip communication in high temperature applications,” in *Embedded Computer Systems: Architectures, Modeling, and Simulation*, Lecture Notes in Computer Science, (Cham), pp. 169–183, Springer International Publishing.
- [34] L. Liu, N. Li, and L. Feng, “Improvement and optimization of lwip,” in *2016 IEEE Advanced Information Management, Communicates, Electronic and Automation Control Conference (IM-CEC)*, pp. 1342–1345, IEEE, 2016.
- [35] FreeRTOS, “Freertos plus tcp - a free thread aware tcp/ip stack for freertos.” https://www.freertos.org/FreeRTOS-Plus/FreeRTOS_Plus_TCP/index.html, Aug 2022.
- [36] H. Nielsen, J. Mogul, L. M. Masinter, R. T. Fielding, J. Gettys, P. J. Leach, and T. Berners-Lee, “Hypertext Transfer Protocol – HTTP/1.1.” RFC 2616, June 1999.
- [37] M. Bishop, “HTTP/3.” RFC 9114, June 2022.

- [38] “7 Series FPGAs Data Sheet: Overview (DS180).” https://docs.xilinx.com/v/u/en-US/ds180_7Series_Overview, Sept. 2020. Standard.
- [39] B. Hinden and D. S. E. Deering, “Internet Protocol, Version 6 (IPv6) Specification.” RFC 2460, Dec. 1998.

Appendix A

Appendix

Write your appendix here. Following two are examples.

A.1 Neov32 memory address space layout

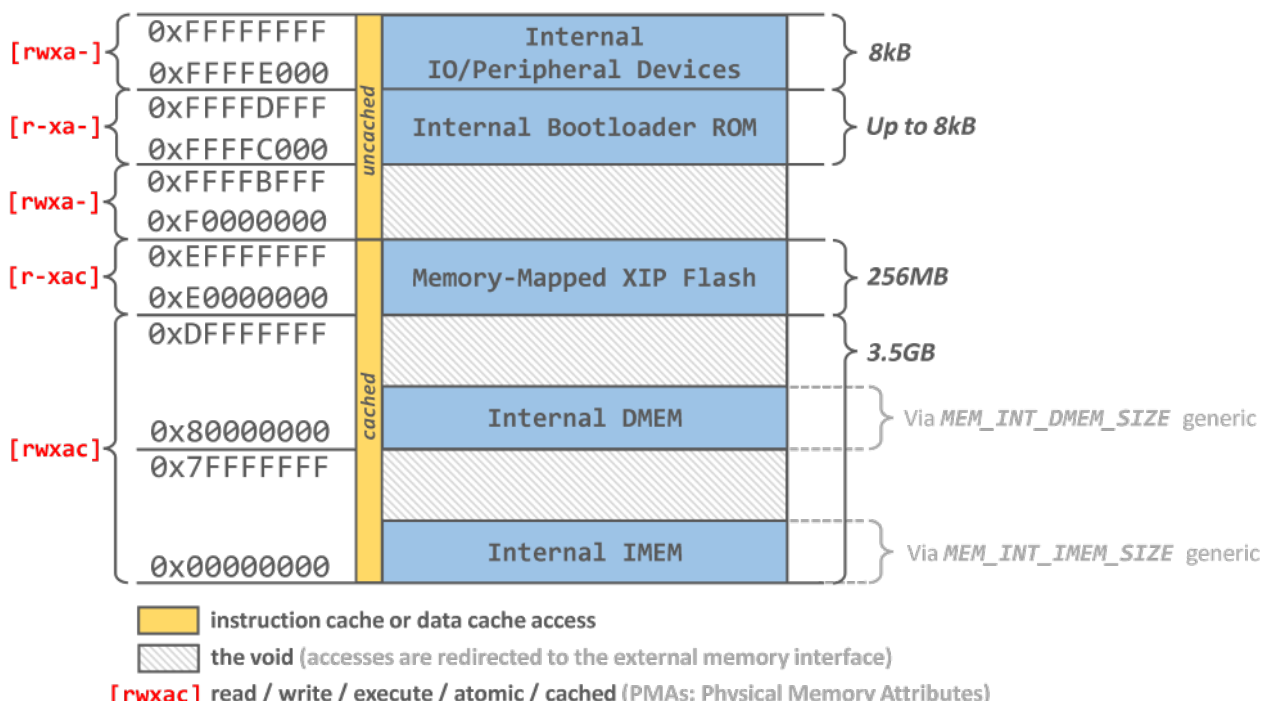


Figure A.1: Neov32 Memory Address space.

Table A.1: FPGA primitives utilisation for XC7A100T

Ref Name	Used	Functional Category
LUT6	16262	LUT
LUT5	14820	LUT
FDRE	14500	Flop & Latch
LUT3	13222	LUT
MUXF7	2436	MuxFx
FDCE	1875	Flop & Latch
RAMD64E	1836	Distributed Memory
LUT4	1294	LUT
LUT2	1016	LUT
MUXF8	884	MuxFx
CARRY4	437	CarryLogic
LUT1	156	LUT
RAMB36E1	130	Block Memory
FDPE	41	Flop & Latch
OBUF	40	IO
LDCE	36	Flop & Latch
IBUF	24	IO
SRLC32E	21	Distributed Memory
OBUFT	11	IO
BUFG	8	Clock
FDSE	5	Flop & Latch
DSP48E1	4	Block Arithmetic
SRL16E	1	Distributed Memory
MMCME2_ADV	1	Clock

Table A.2: Memory Utilisation

Site Type	Used	Fixed	Prohibited	Available	Util%
Block RAM Tile	130	0	0	135	96.30
RAMB36/FIFO*	130	0	0	135	96.30
RAMB36E1 only	130	-	-	-	-
RAMB18	0	0	0	270	0.00

Table A.3: Slice Logic Utilisation

Site Type	Used	Fixed	Prohibited	Available	Util%
Slice LUTs*	40920	0	0	63400	64.54
LUT as Logic	39062	0	0	63400	61.61
LUT as Memory	1858	0	0	19000	9.78
LUT as Distributed RAM	1836	-	-	-	-
LUT as Shift Register	22	-	-	-	-
Slice Registers	16457	0	0	126800	12.98
Register as Flip Flop	16421	0	0	126800	12.95
Register as Latch	36	0	0	126800	0.03
F7 Muxes	2436	0	0	31700	7.68
F8 Muxes	884	0	0	15850	5.58

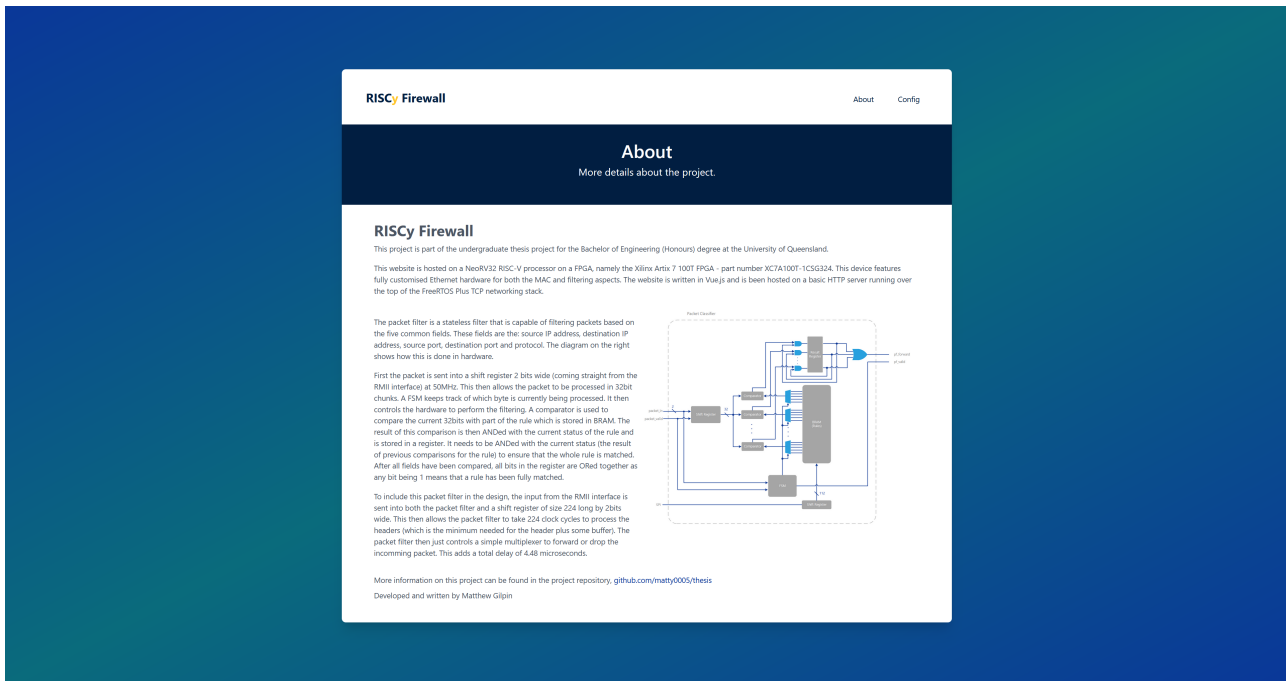


Figure A.2: Screenshot of the about page in the webapp.

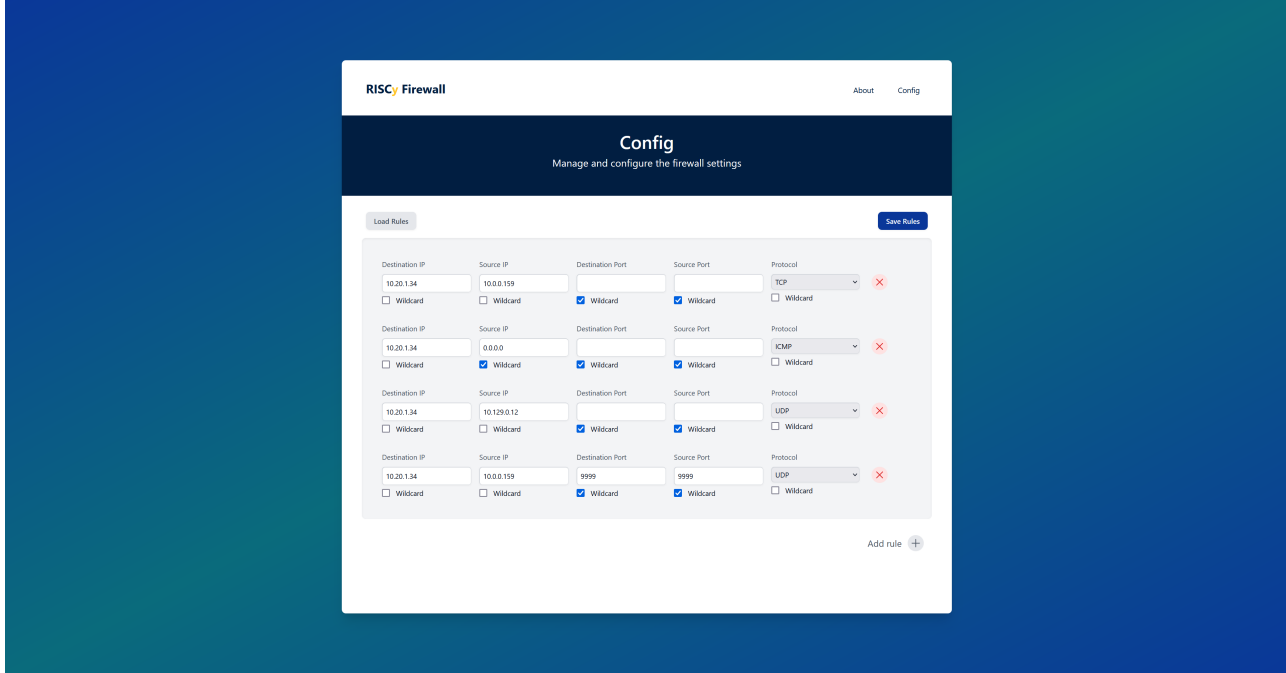


Figure A.3: Screenshot of the config page in the webapp.

Table A.4: Average UDP RTT for different devices and payload sizes.

Device	8 bytes (ms)	256 bytes (ms)
WIZ5500 Pico	1.88	2.07
F767ZI	1.30	1.39
F767ZI 80Mhz	1.41	1.51
MilkV	1.04	1.09
FPGA board	1.45	1.72

A.2 FPGA primitives utilisation

A.3 Additional webpages built into the webserver.

A.4 UDP ping times between boards

A.5 Current measurements from boards

Table A.5 shows the current measurements. Notably Diff1 is the difference between the Idle and No ETH fields while Diff2 is the difference between the Idle and Clean states.

Table A.5: Device power consumption data (all values in mA)

Device	Idle	Busy	Average	No ETH	Clean	Diff1	Diff2
FPGA	301.4	300.13	300.765	264	202.13	37.4	99.27
MilkV	76.27	76.53	76.4	69.23	69.23	7.04	7.04
F767ZI	209.25	206.9	208.075	153.46	121.31	55.79	87.94
WIZ5500	155.88	158.67	157.275	97.9	80.35	57.98	75.53

A.6 Thermal measurements for boards

Table A.6: Device measurements over time using FLIR One thermal camera, all measurements in degrees Celsius.

Device	5min	10min	30min	1h	2h
FPGA	38	38.2	38.9	39.1	40.4
MilkV	36.7	39.8	35.5	39.1	38.1
F767ZI (STM)	35.9	38.9	35.8	37.5	36.8
F767ZI (PHY)	38	38.8	35.2	37.2	36.2
WIZ5500 (RP2040)	46.6	53.1	54.6	54.5	53.2
WIZ5500 (PHY)	58	59	58.4	58.5	56.8

A.7 Testing the firewall with 4 nodes.

Node 1

```

1 pi@node1:~/thesis-tools $ python3 test.py
2 Testing from IP: 10.20.1.10
3 Ping to 10.20.1.34 took 0.522 ms
4 TCP (10.20.1.34, 1337) received response in 1.02ms: e5 07 00 00
5 UDP (10.20.1.34, 1337) received response from ('10.20.1.34', 1337) in
   0.83ms: egasseM llawerif yCSIR
6 UDP (10.20.1.34, 9999) received response from ('10.20.1.34', 9999) in
   1.41ms: ok
7 Failed to retrieve content from http://10.20.1.34/

```

Node 2

```

8 pi@node2:~/thesis-tools $ python3 test.py
9 Testing from IP: 10.20.1.11
10 Ping to 10.20.1.34 took 1.12 ms
11 TCP: (10.20.1.34, 1337) Error occurred: timed out
12 UDP: (10.20.1.34, 1337) Error occurred: timed out
13 UDP (10.20.1.34, 9999) received response from ('10.20.1.34', 9999) in
   1.08ms: ok
14 Failed to retrieve content from http://10.20.1.34/

```

Node 3

```

15 matt@Node3:~/thesis-tools$ python3 test.py
16 Testing from IP: 10.0.0.5
17 Ping to 10.20.1.34 took 0.979 ms
18 TCP: (10.20.1.34, 1337) Error occurred: timed out
19 UDP (10.20.1.34, 1337) received response from ('10.20.1.34', 1337) in
   1.45ms: egasseM llawerif yCSIR
20 UDP (10.20.1.34, 9999) received response from ('10.20.1.34', 9999) in
   1.70ms: ok
21 HTTP received from http://10.20.1.34/:80 in 11.95ms

```

Node 4

```

22 matt@Node4:~/thesis-tools $ python3 test.py

```

```

23 Testing from IP: 10.0.0.93
24 Ping to 10.20.1.34 took 1.23 ms
25 TCP (10.20.1.34, 1337) received response in 1.11ms: e5 07 00 00
26 UDP: (10.20.1.34, 1337) Error occurred: timed out
27 UDP (10.20.1.34, 9999) received response from ('10.20.1.34', 9999) in
   1.10ms: ok
28 Failed to retrieve content from http://10.20.1.34/

```

A.8 Iperf 3 Test results

```

matt:FreeRTOS$ iperf3 -c 10.20.1.120 -p 5001
Connecting to host 10.20.1.120, port 5001
[ 5] local 172.28.174.202 port 52200 connected to 10.20.1.120 port 5001
[ ID] Interval          Transfer     Bitrate      Retr  Cwnd
[ 5]  0.00-1.00  sec   87.5 KBytes   716 Kbits/sec   33  1.37 KBytes
[ 5]  1.00-2.00  sec   164 KBytes   1.34 Mbits/sec   42  1.37 KBytes
[ 5]  2.00-3.00  sec   180 KBytes   1.48 Mbits/sec   41  1.37 KBytes
[ 5]  3.00-4.00  sec   164 KBytes   1.34 Mbits/sec   42  1.37 KBytes
[ 5]  4.00-5.00  sec   164 KBytes   1.34 Mbits/sec   41  1.37 KBytes
[ 5]  5.00-6.00  sec   180 KBytes   1.48 Mbits/sec   41  1.37 KBytes
[ 5]  6.00-7.00  sec   164 KBytes   1.34 Mbits/sec   40  1.37 KBytes
[ 5]  7.00-8.00  sec   164 KBytes   1.34 Mbits/sec   41  1.37 KBytes
[ 5]  8.00-9.00  sec   164 KBytes   1.34 Mbits/sec   41  2.73 KBytes
[ 5]  9.00-10.00 sec   180 KBytes   1.48 Mbits/sec   42  1.37 KBytes
- - - - - [ ID] Interval          Transfer     Bitrate      Retr
[ 5]  0.00-10.00 sec  1.58 MBytes   1.32 Mbits/sec  404                     sender
[ 5]  0.00-10.00 sec  1.58 MBytes   1.32 Mbits/sec                     receiver
iperf Done.

```

Figure A.4: Nexys A7 and designed hardware Iperf3 test results.

A.9 Eye Diagrams of PMOD port

```
matt:thesis-tools$ iperf -c 10.20.1.22 -i 1
-----
Client connecting to 10.20.1.22, TCP port 5001
TCP window size: 45.0 KByte (default)
-----
[ 1] local 172.28.174.202 port 52888 connected with 10.20.1.22 port 5001
[ ID] Interval      Transfer     Bandwidth
[ 1] 0.0000-1.0000 sec   768 KBytes  6.29 Mbits/sec
[ 1] 1.0000-2.0000 sec   896 KBytes  7.34 Mbits/sec
[ 1] 2.0000-3.0000 sec   896 KBytes  7.34 Mbits/sec
[ 1] 3.0000-4.0000 sec   896 KBytes  7.34 Mbits/sec
[ 1] 4.0000-5.0000 sec   896 KBytes  7.34 Mbits/sec
[ 1] 5.0000-6.0000 sec   768 KBytes  6.29 Mbits/sec
[ 1] 6.0000-7.0000 sec   896 KBytes  7.34 Mbits/sec
[ 1] 7.0000-8.0000 sec   896 KBytes  7.34 Mbits/sec
[ 1] 8.0000-9.0000 sec   896 KBytes  7.34 Mbits/sec
[ 1] 9.0000-10.0000 sec  768 KBytes  6.29 Mbits/sec
[ 1] 0.0000-10.0270 sec  8.50 MBytes  7.11 Mbits/sec
matt:thesis-tools$
```

Figure A.5: Nucleo-F767ZI Iperf3 test results.

```
matt:~$ iperf3 -c 10.20.1.31
Connecting to host 10.20.1.31, port 5201
[ 5] local 172.28.174.202 port 54242 connected to 10.20.1.31 port 5201
[ ID] Interval      Transfer     Bitrate      Retr  Cwnd
[ 5]  0.00-1.00    sec   11.3 MBytes  94.5 Mbits/sec  315  19.8 KBytes
[ 5]  1.00-2.00    sec   10.9 MBytes  91.7 Mbits/sec  305  21.2 KBytes
[ 5]  2.00-3.00    sec   10.9 MBytes  91.7 Mbits/sec  303  24.0 KBytes
[ 5]  3.00-4.00    sec   10.9 MBytes  91.7 Mbits/sec  319  22.6 KBytes
[ 5]  4.00-5.00    sec   10.9 MBytes  91.3 Mbits/sec  315  32.5 KBytes
[ 5]  5.00-6.00    sec   10.9 MBytes  91.3 Mbits/sec  326  24.0 KBytes
[ 5]  6.00-7.00    sec   11.2 MBytes  94.0 Mbits/sec  315  21.2 KBytes
[ 5]  7.00-8.00    sec   10.9 MBytes  91.7 Mbits/sec  330  24.0 KBytes
[ 5]  8.00-9.00    sec   11.1 MBytes  93.1 Mbits/sec  305  26.9 KBytes
[ 5]  9.00-10.00   sec   11.1 MBytes  93.1 Mbits/sec  356  26.9 KBytes
-----
[ ID] Interval      Transfer     Bitrate      Retr
[ 5]  0.00-10.00   sec   110 MBytes  92.4 Mbits/sec  3189
[ 5]  0.00-10.04   sec   110 MBytes  91.8 Mbits/sec
                                                               sender
                                                               receiver
iperf Done.
matt:~$ |
```

Figure A.6: MilkV-duo Iperf3 test results.

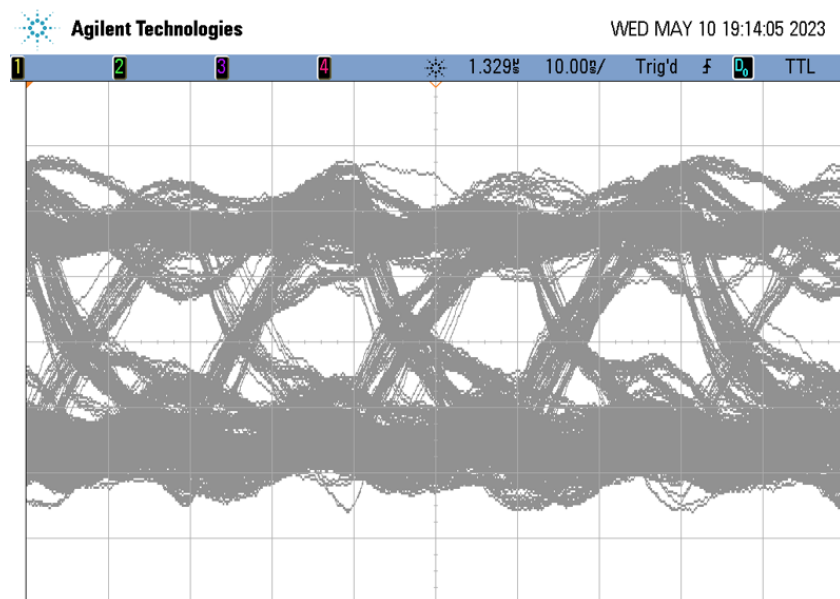


Figure A.7: Eye diagram of TXD through PMOD interface.